

# Mitochondrial dysfunction induces triglyceride accumulation in 3T3-L1 cells: role of fatty acid $\beta$ -oxidation and glucose

Sébastien Vankoningsloo, Marie Piens, Christophe Lecocq, Audrey Gilson, Aurélie De Pauw, Patricia Renard, Catherine Demazy, Andrée Houbion, Martine Raes, and Thierry Arnould<sup>1</sup>

Laboratory of Biochemistry and Cellular Biology, University of Namur, 5000 Namur, Belgium

**Abstract** Mitochondrial cytopathy has been associated with modifications of lipid metabolism in various situations, such as the acquisition of an abnormal adipocyte phenotype observed in multiple symmetrical lipomatosis or triglyceride (TG) accumulation in muscles associated with the myoclonic epilepsy with ragged red fibers syndrome. However, the molecular signaling leading to fat metabolism dysregulation in cells with impaired mitochondrial activity is still poorly understood. Here, we found that preadipocytes incubated with inhibitors of mitochondrial respiration such as antimycin A (AA) accumulate TG vesicles but do not acquire specific markers of adipocytes. Although the uptake of TG precursors is not stimulated in 3T3-L1 cells with impaired mitochondrial activity, we found a strong stimulation of glucose uptake in AA-treated cells mediated by calcium and phosphatidylinositol 3-kinase/Akt1/glycogen synthase kinase 3 $\beta$ , a pathway known to trigger the translocation of glucose transporter 4 to the plasma membrane in response to insulin. TG accumulation in AA-treated cells is mediated by a reduced peroxisome proliferator-activated receptor  $\gamma$  activity that downregulates muscle carnitine palmitoyl transferase-1 expression and fatty acid  $\beta$ -oxidation, and by a direct conversion of glucose into TGs accompanied by the activation of carbohydrate-responsive element binding protein, a lipogenic transcription factor. Taken together, these results could explain how mitochondrial impairment leads to the multivesicular phenotype found in some mitochondria-originating diseases associated with a dysfunction in fat metabolism.—Vankoningsloo, S., M. Piens, C. Lecocq, A. Gilson, A. De Pauw, P. Renard, C. Demazy, A. Houbion, M. Raes, and T. Arnould. Mitochondrial dysfunction induces triglyceride accumulation in 3T3-L1 cells: role of fatty acid  $\beta$ -oxidation and glucose. *J. Lipid Res.* 2005. 46: 1133–1149.

**Supplementary key words** muscle carnitine palmitoyl transferase-1 • phosphatidylinositol 3-kinase/Akt1/glycogen synthase kinase 3 $\beta$  • AMP-dependent kinase • carbohydrate-responsive element binding protein • peroxisome proliferator-activated receptor  $\gamma$

The role of mitochondria in lipid homeostasis has been strongly emphasized in recent studies focusing on mitochondrial respiratory deficiency. Indeed, chronic mitochondrial dysfunction can lead to diseases characterized by lipid metabolism disorders and pathological triglyceride (TG) accumulation in several cell types (1–3). Genetic mitochondrial pathologies usually result from point mutations or deletions in mitochondrial DNA that finally impair oxidative phosphorylation capacity (4). Interestingly, some mitochondrial disorders affect lipid-metabolizing tissues such as muscular and adipose tissues. For example, the myoclonic epilepsy with ragged red fibers (MERRF) syndrome, commonly caused by a point mutation in the mitochondrial tRNA<sup>Lys</sup>-encoding gene (A8344G), is associated with myopathy, TG accumulation in muscles (5), and, in some cases, multiple symmetrical lipomatosis (MSL) (2, 6). MSL is a pathology characterized by the formation of lipomas containing abnormal white adipocytes smaller than normal adipocytes showing a multivesicular phenotype (1, 2, 7). Moreover, biochemical analyses have shown that cytochrome *c* oxidase activity is impaired in muscles from patients with MSL (8), supporting the fact that the disease is linked to mitochondrial dysfunction (6, 9). The role of mitochondria in the lipid metabolism of white adipose tissue was also strengthened in the pathogenesis of

Abbreviations: AA, antimycin A; ACC, acetyl-coenzyme A carboxylase; AICAR, 5-aminoimidazole-4-carboxamide-1- $\beta$ -D-ribofuranoside; AMPK, AMP-dependent kinase; BAPTA-AM, 1,2-bis(2-aminophenoxy)ethane-*N,N,N',N'*-tetraacetic acid; C/EBP $\beta$ , CCAAT/enhancer-binding protein  $\beta$ ; ChREBP, carbohydrate-responsive element binding protein; 2-DG, 2-deoxy-D-[3H]glucose; EGCG, (–)-epigallocatechin gallate; FABP4, fatty acid binding protein 4; FCCP, carbonyl cyanide (*p*-trifluoromethoxy)phenylhydrazine; FCS, fetal calf serum; GLUT, glucose transporter; GSK3 $\beta$ , glycogen synthase kinase 3 $\beta$ ; HB, hypotonic buffer; IRS-1, insulin receptor substrate-1; L-PK, liver pyruvate kinase; M-CPT-1, muscle carnitine palmitoyl transferase-1; MERRF, myoclonic epilepsy with ragged red fibers; MSL, multiple symmetrical lipomatosis; NAC, *N*-acetyl-L-cysteine; PI 3-kinase, phosphatidylinositol 3-kinase; PPAR $\gamma$ , peroxisome proliferator-activated receptor  $\gamma$ ; ROS, reactive oxygen species; RXR $\alpha$ , retinoid X receptor  $\alpha$ ; TBP, TATA box binding protein; TG, triglyceride; UCP-2, uncoupling protein-2.

<sup>1</sup> To whom correspondence should be addressed.  
e-mail: thierry.arnould@fundp.ac.be

Manuscript received 19 November 2004 and in revised form 25 January 2005 and in re-revised form 15 February 2005.

Published, JLR Papers in Press, March 1, 2005.  
DOI 10.1194/jlr.M400464JLR200

lipodystrophy syndromes induced by highly active anti-retroviral therapies known to impair mitochondrial functions (3).

These various lipid disorders suggest a strong link between mitochondrial dysfunction and fat storage abnormalities. However, despite the numerous case reports with histological observations (1), the role of mitochondrial activity in adipose tissue and the molecular mechanisms by which mitochondrial impairment can lead to cellular accumulation of TG are still poorly understood. Besides the key role of mitochondria in cellular functions, such as ATP production and participation to numerous synthetic pathways, impaired mitochondria generate reactive oxygen species (ROS) acting as messengers, for example, to inhibit adipocyte differentiation by controlling the expression of the adipogenic repressor CHOP10/GADD153 (10).

Previously, we and others demonstrated that the increase of calcium concentration in response to mitochondrial activity inhibition also modifies the activity of transcription factors and gene expression (11–13). To identify the mechanisms involved in TG accumulation in response to mitochondrial dysfunction, we used 3T3-L1 preadipocytes to study the effects of mitochondrial activity deficiency on lipid metabolism. We particularly focused our investigation on two major metabolic pathways: glucose metabolism and fatty acid  $\beta$ -oxidation. Here, we found that TG accumulation in preadipocytes in response to mitochondrial activity inhibition involves both a reduction of fatty acid  $\beta$ -oxidation and a major role for massively imported glucose through a phosphatidylinositol 3-kinase (PI 3-kinase)/Akt1/glycogen synthase kinase 3 $\beta$  (GSK3 $\beta$ ) pathway that results in glucose transporter 4 (GLUT4) translocation to the plasma membrane.

## MATERIALS AND METHODS

### Chemicals

The different molecules and inhibitors, such as antimycin A (AA), myxothiazol, oligomycin, rotenone, carbonyl cyanide (*p*-trifluoromethoxy)phenylhydrazone (FCCP), (–)-epigallocatechin gallate (EGCG), 1,2-bis(2-aminophenoxy)ethane-*N,N,N',N'*-tetraacetic acid (BAPTA-AM), cytochalasin B, *N*-acetyl-L-cysteine (NAC), dibutyryl cAMP, dexamethasone, dextrine, Oil Red O, propidium iodide, and SB216763, were purchased from Sigma. Stigmatellin was bought from Fluka, LY294002 and wortmannin from Biomol, insulin from Gibco BRL, and the protease inhibitor cocktail from Roche.

### Cell culture conditions and experimental models

3T3-L1 mouse preadipocytes, purchased from the American Type Culture Collection, were cultivated in DHG medium [Dulbecco's modified Eagle's medium + high glucose (4.5 g/l); Gibco BRL] supplemented with 10% fetal calf serum (FCS; Gibco BRL). Cells were incubated in a 5% CO<sub>2</sub> incubator in a humidified atmosphere. For preadipocyte differentiation, 3T3-L1 cells were seeded at 50% confluence 3 days before the beginning of the differentiation program. Confluent cell monolayers (day 0) were switched for 48 h to media containing the adipogenic cocktail (DHG-L1 medium, which is DHG that contains 1.5 g/l NaHCO<sub>3</sub>) supplemented with 10% FCS, 5  $\mu$ g/ml insulin, 300  $\mu$ M dibutyryl

cAMP, and 1  $\mu$ M dexamethasone. When needed, cells were then refed every other day with DHG-L1 containing 10% FCS and 5  $\mu$ g/ml insulin. To trigger a prolonged mitochondrial inhibition, confluent cells (day 0) were incubated in DHG-L1 containing 10% FCS with or without the different mitochondrial inhibitors. When cell cultures were maintained for more than 2 days after day 0, media were replaced every other day by DHG-L1 containing 10% FCS and the inhibitor of interest at the same concentration. Where indicated, some inhibitors were added during the whole program or in preincubation for several hours before the assays.

### TG staining and quantitative analysis

Oil Red O at 0.2% in isopropyl alcohol was mixed with dextrine at 1% in water (3:2, v/v) and filtered. At the end of the different incubations, cultured cells on 24-well plates (Corning) were washed with PBS, fixed for 2 min with 0.5 ml of paraformaldehyde (Sigma) at 3.7% in PBS, incubated for 30 min with 0.5 ml of Oil Red O, and washed twice with PBS. Absorbance of cell monolayers at 490 nm was then measured in a spectrophotometer (Ultramark; Bio-Rad), and stained TGs were visualized by phase-contrast microscopy. In some conditions, TG content was normalized for total DNA content, as determined by iodide propidium staining; cells were then permeabilized for 30 min with 0.5 ml of 100% ethanol and incubated for 30 min with 0.5 ml of propidium iodide at 10  $\mu$ g/ml in PBS. Fluorescence (excitation, 515 nm; emission, 612 nm) was then measured with a spectrofluorimeter (FluoStar; BMG). For quantitative assays, TG content was determined after lipid extraction with the INT kit (Sigma). Briefly, cells were maintained in 25 cm<sup>2</sup> flasks (Corning) for 8 days with or without AA, FCCP, or the adipogenic cocktail, scraped in 3 ml of CH<sub>3</sub>OH/water (2:0.8, v/v), and TGs were extracted with 1 ml of CHCl<sub>3</sub>. The aqueous phase was washed with 1 ml of CHCl<sub>3</sub>, solvent was evaporated, and TGs were resuspended in 300  $\mu$ l of CHCl<sub>3</sub>/CH<sub>3</sub>OH (2:1, v/v) and quantified with the INT kit according to the manufacturer's instructions.

### TG precursor uptake and fatty acid $\beta$ -oxidation assays

Cells were seeded at 50% confluence on 12-well plates (Corning) 3 days before incubation (day 0) with the adipogenic cocktail, AA, or FCCP. Cells were then washed with PBS/0.5% BSA (Sigma), incubated at 37°C for 90 min with 1  $\mu$ Ci/ml [<sup>3</sup>H]glycerol (New England Nuclear) and 1  $\mu$ Ci/ml [<sup>14</sup>C]oleate (New England Nuclear) in DHG-L1 medium containing 0.5% BSA, washed twice with PBS/0.5% BSA, and finally lysed in 200  $\mu$ l of 0.5 N NaOH. After neutralization, radioactivity was counted with a liquid scintillation analyzer and normalized for protein content (14). Fatty acid  $\beta$ -oxidation rate was assessed in 3T3-L1 cells incubated for 8 days with the adipogenic cocktail, AA, or FCCP by the release of <sup>14</sup>CO<sub>2</sub> after [<sup>14</sup>C]oleate uptake as described previously (15). In some conditions, cells were preincubated for 180 min with or without 500  $\mu$ M 5-aminoimidazole-4-carboxamide-1- $\beta$ -D-ribofuranoside (AICAR; Toronto Research Center) before the assay.

### Real-time PCR determination of carnitine palmitoyl transferase-1 mRNA steady-state levels

3T3-L1 cells were incubated or not for 8 days with AA, with ciglitazone (Biomol) and 9-*cis*-retinoic acid (Biomol), or with a combination of these molecules. At the end of the incubations, total RNA was extracted with the RNeasy Total RNA Isolation System (Promega), and 1  $\mu$ g was engaged in reverse transcription using random priming and Superscript II reverse transcriptase (Invitrogen) according to the manufacturer's instructions. Quantitative real-time PCR was performed by monitoring the increase in fluorescence of incorporated SYBR Green dye with an ABI PRISM 7000 Sequence Detector System (Applied Biosystem). Spe-

cific primers for muscle carnitine palmitoyl transferase-1 (M-CPT-1; forward, 5'-CTCCAGCAAATACTCAAGTTCAGAGA-3'; reverse, 5'-TTCCTCAGCTGTCTGTCTTGGAA-3'), for liver CPT-1 (forward, 5'-GCGCTCTTAGGACTACTTGCTAACCC-3'; reverse, 5'-ACTGGA-GACCTGAGAGAGGAATGT-3'), and for TATA box binding protein (TBP)/Transcription Factor IID complex (forward, 5'-CAGTT-ACAGGTGGCAGCATGA-3'; reverse, 5'-TAGTGCTGCAGGGTGA-TTTCAG-3') were designed using Primer Express software (Applied Biosystem). TBP/TFIID was used for normalization and relative mRNA quantification.

### Nuclear protein extraction and peroxisome proliferator-activated receptor $\gamma$ /retinoid X receptor $\alpha$ DNA binding assay

Nuclear protein extractions in high-salt buffer were prepared as described previously (16). Briefly, cultured 3T3-L1 cells in 75 cm<sup>2</sup> flasks (Corning) were incubated on ice for 3 min with 10 ml of cold hypotonic buffer (HB; 20 mM HEPES, 5 mM NaF, 1 mM Na<sub>2</sub>MoO<sub>4</sub>, and 0.1 mM EDTA) and harvested in 500  $\mu$ l of HB containing 0.2% Nonidet P-40 (Sigma), protease inhibitors (Roche), and phosphatase inhibitors (1 mM Na<sub>3</sub>VO<sub>4</sub>, 5 mM NaF, 10 mM *p*-nitrophenylphosphate, and 10 mM  $\beta$ -glycerophosphate). Cell lysates were centrifuged for 30 s at 13,000 rpm, and the sedimented nuclei were resuspended in 50  $\mu$ l of HB containing 20% glycerol and protease/phosphatase inhibitors. High-saline extraction was performed by the addition of 100  $\mu$ l of HB containing 20% glycerol, 0.8 M NaCl, and protease/phosphatase inhibitors. Aliquots were frozen at -70°C, and protein concentrations were determined (14). DNA binding assays were performed with the TransAM kit (Active Motif) according to the manufacturer's instructions. Briefly, 5  $\mu$ g of nuclear proteins was incubated for 2 h on a 96-well plate coated with a double-stranded oligonucleotide containing the consensus sequence for peroxisome proliferator-activated receptor  $\gamma$  (PPAR $\gamma$ ; DR-1, AGGTCAAAGGTC). DNA binding activity was detected with either an anti-PPAR $\gamma$  or an anti-retinoid X receptor  $\alpha$  (RXR $\alpha$ ) antibody (Santa Cruz) and revealed by a colorimetric reaction with HRP-conjugated secondary antibodies. The enzymatic reaction was stopped and absorbance was measured at 450 nm with a spectrophotometer (Bio-Rad).

### Western blot analysis

3T3-L1 cells were collected in 1 ml of cold lysis buffer (20 mM Tris, pH 7.4, 150 mM NaCl, 1 mM EDTA, 1% Triton X-100, and protease/phosphatase inhibitors). Clear lysates were prepared and sample protein contents were determined by the bicinchoninic acid method (Pierce). For GLUT4 immunoblotting, crude plasma membranes were prepared as described previously (17). Twenty micrograms of proteins was resolved by SDS-PAGE (10%) and electroblotted onto polyvinylidene difluoride membranes (Millipore). Membranes were blocked for 2 h at room temperature in TBS-T (20 mM Tris, pH 7.4, 150 mM NaCl, and 0.1% Tween 20) with 5% nonfat milk (Gloria) and incubated for 1 h at room temperature with an anti-fatty acid binding protein 4 (FABP4)/adipose fatty acid binding protein (aP2), an anti-PPAR $\gamma$  (Santa Cruz), anti-uncoupling protein-2 (UCP-2; Santa Cruz), an anti-CCAAT/enhancer-binding protein  $\beta$  (C/EBP $\beta$ ; Santa Cruz), or an anti-GLUT4 (Santa Cruz) antibody at 1  $\mu$ g/ml in the same buffer. For the detection of phosphorylated acetyl-coenzyme A carboxylase (ACC), membrane was blocked for 2 h in TBS containing 5% nonfat milk, 5% BSA (Sigma), and 0.07% Tween 20 and then incubated for 16 h at 4°C with an anti-Ser79-phosphorylated ACC antibody (Upstate) at 1  $\mu$ g/ml in the same buffer. The abundance of immunoprecipitated GSK3 $\beta$  was analyzed with an anti-GSK3 $\beta$  monoclonal antibody (Santa Cruz; 1  $\mu$ g/ml). Immunostained proteins were visualized using a HRP-conjugated antibody (Dako) and the enhanced chemiluminescence detection system (Pierce).

### Mammalian cell transient transfection and luciferase assay

3T3-L1 cells seeded on 12-well plates were transiently cotransfected for 6 h with the SuperFect reagent (Qiagen; ratio, 1:5) with a luciferase reporter construct (0.75  $\mu$ g/well) driven either by a synthetic promoter containing three PPAR responsive element (PPRE) sites (tk-PPREx3-Luc) or by the carbohydrate-responsive element binding protein (ChREBP)-sensitive liver pyruvate kinase (L-PK) promoter, together with a cytomegalovirus promoter/ $\beta$ -galactosidase expression plasmid (0.25  $\mu$ g/well; Clontech). Where indicated, cells were cotransfected with 0.25  $\mu$ g/well of a construct encoding PPAR $\gamma$ 2 (pSV-SPORT PPAR $\gamma$ 2). Cells were then incubated with the adipogenic cocktail, mitochondrial inhibitors, or PPAR $\gamma$  activators for 24 or 48 h. Luciferase activity in cell lysates was determined using the reporter assay system (Promega) and normalized for  $\beta$ -galactosidase activity.

### Glucose uptake

Cells were incubated with the different molecules for 48 h, washed with PBS, and incubated for 30 min with PBS containing 1  $\mu$ Ci/ml 2-deoxy-D-[<sup>3</sup>H]glucose (Perkin Elmer). Cells were then rinsed twice with PBS and lysed with 200  $\mu$ l of 0.5 N NaOH. After neutralization, radioactivity was counted and results were normalized for protein content (14). Where indicated, cells were preincubated for 4 h with cytochalasin B or for 3 h with BAPTA-AM, LY294002, NAC, SB216763, or AICAR before the glucose uptake assay. In some experiments, 3T3-L1 cells were transfected by electroporation with a Nucleofector system (Amaxa) according to the manufacturer's instructions. Briefly, cells were electroporated (U-24 program; 100  $\mu$ l of R solution per well) in the presence of 5  $\mu$ g of an expression vector encoding either an AMP-dependent kinase (AMPK) dominant negative form or green fluorescent protein. Cells were then plated on six-well plates (300,000 cells/well) and incubated for 48 h with 10 nM AA before glucose uptake was assessed.

### Glucose-to-TG conversion assay

Cells were seeded at 50% confluence in 25 cm<sup>2</sup> flasks (Corning) and 3 days later were incubated or not for 8 days with 10 nM AA and then for 90 min with 1.5  $\mu$ Ci/ml (5  $\mu$ M) glucose D-[<sup>14</sup>C(U)] (303 mCi/mmol; Perkin Elmer). TGs were extracted as described above, and <sup>14</sup>C radioactivity associated with lipids was counted on an aliquot with a liquid scintillation analyzer (TRI-CARB-2100TR; Packard). Results were then normalized for protein content (14).

### Immunofluorescence staining and confocal microscopy

For C/EBP $\beta$ , p110 $\alpha$ , phosphorylated Akt1, and phosphorylated AMPK immunostaining, cells were seeded on cover slips and incubated for 24 or 48 h with the adipogenic cocktail or 10 nM AA, fixed for 10 min with 4% paraformaldehyde, permeabilized for 5 min with PBS/1% Triton X-100, and then incubated for 2 h with an anti-C/EBP $\beta$  (Santa Cruz) or an anti-p110 $\alpha$  (Upstate) antibody or for 16 h at 4°C with an anti-pSer473-Akt1 (Cell Signaling), an anti-pThr308-Akt1 (Cell Signaling), or an anti-pThr172-AMPK (Cell Signaling) antibody diluted 40 times in PBS/1% BSA. Where indicated, cells were preincubated or not for 2 h in the presence of 10  $\mu$ M BAPTA-AM before immunostaining. Finally, cells were incubated for 1 h at room temperature with an Alexa-labeled secondary antibody (Molecular Probes) diluted 500 times in PBS/1% BSA and processed for confocal microscopy (Leica). In some conditions, nuclei were visualized by ToPro-3 staining.

### Quantitative total Akt and phosphorylated Akt detection

The detection of Akt and the Ser473-phosphorylated form was performed using the total and pSer473-Akt detection kits (Biosource International). 3T3-L1 cells were first incubated with the



adipogenic cocktail, AA, or FCCP for 1, 6, 24, or 48 h and lysed, and 10  $\mu$ g of proteins was assayed for both total Akt and pSer473-Akt according to the manufacturer's instructions.

### GSK3 $\beta$ kinase assay

Confluent 3T3-L1 cells were incubated for 48 h with or without 10 nM AA. Cells were then lysed in 1 ml of cold lysis buffer containing 1% Triton X-100, 150 mM NaCl, 10 mM Tris-HCl, pH 7.5, 1 mM EDTA, 1 mM EGTA, 1 mM Na<sub>3</sub>VO<sub>4</sub>, and a protease inhibitor cocktail (Roche). GSK3 $\beta$  was then immunoprecipitated from cleared lysates with 5  $\mu$ g of a monoclonal anti-GSK3 $\beta$  antibody (Transduction Laboratories) for 2 h at 4°C. Immune complexes were immobilized by adding 60  $\mu$ l of Protein G Plus/Protein A-Agarose beads (Oncogene) and washed twice with 800  $\mu$ l of lysis buffer. For the determination of immunoprecipitated kinase, aliquots of resuspended beads were resolved by 10% SDS-PAGE and Western blot analysis. Immunoprecipitates were washed with 500  $\mu$ l of kinase reaction buffer (20 mM Tris-HCl, pH 7.5, 10 mM MgCl<sub>2</sub>, and 5 mM dithiothreitol) and resuspended in 50  $\mu$ l of kinase reaction buffer containing 50  $\mu$ M cAMP-responsive element binding phosphopeptide (New England Biolabs). The assay was carried out in the presence of 20  $\mu$ M unlabeled ATP (Sigma) and 10  $\mu$ Ci of [ $\gamma$ -<sup>32</sup>P]ATP (Perkin Elmer) for 30 min at 30°C. In some conditions, lithium acetate (40  $\mu$ M) was added before the assay. A 25  $\mu$ l aliquot was applied to a phosphocellulose membrane spin column (Pierce) and washed with 500  $\mu$ l of 75 mM H<sub>3</sub>PO<sub>4</sub>, and membrane-associated radioactivity was counted.

### Statistical analysis

Data were analyzed by ANOVA I and Sheffe's contrasts. Differences between tests and controls were considered statistically significant at  $P < 0.05$  or less.

## RESULTS

### Metabolic mitochondrial inhibitors that impair respiration trigger TG accumulation in 3T3-L1 cells

We first observed that rotenone (complex I inhibitor), AA, stigmatellin, myxothiazol (molecules that inhibit complex III), and oligomycin (F<sub>0</sub>-F<sub>1</sub> ATP synthase inhibitor) induce TG accumulation in 3T3-L1 cells in a dose-dependent manner, as visualized after Oil Red O staining for neutral lipids and illustrated for cells incubated with AA for 8 days (Fig. 1A). The formation of numerous cytosolic TG vesicles in cells treated with various mitochondrial inhibitors or in differentiated adipocytes is indicated by Oil Red O staining and phase-contrast microscopy observations, whereas the uncoupler FCCP does not increase cellular TG content (Fig. 1B). TGs form larger but less abundant vesicles in 3T3-L1 cells differentiated with a standard adipogenic cocktail. In addition, the differentiating 3T3-L1 cells display hypertrophy and round shape, whereas cells treated with mitochondrial inhibitors keep a fibroblastic phenotype (Fig. 1B). TG accumulation in AA-treated 3T3-L1 cells is time- (Fig. 1C) and concentration-dependent (data not shown), as measured by Oil Red O staining and spectrophotometric determination. Significant TG accumulation in 3T3-L1 cells treated with 10 nM AA is observed after 8 days of incubation but never exceeds 30% to 40% of TGs that accumulate in differentiated cells. To take cell number into account in the different condi-

tions, we compared TG accumulation in AA-treated cells normalized or not for total DNA content determined by propidium iodide staining and found similar results (Fig. 1D, E).

Cellular TG accumulation has also been confirmed using a quantitative TG INT reagent kit. After 8 days of treatment and when normalized for protein content, we compared amounts of TG in control cells, in cells treated with 10 nM AA, in differentiated cells, and in cells incubated with 1  $\mu$ M FCCP and found  $0.31 \pm 0.06$ ,  $0.82 \pm 0.08$  ( $P < 0.05$ ),  $1.55 \pm 0.57$  ( $P < 0.001$ ), and  $0.41 \pm 0.15$  mg TG/mg proteins, respectively ( $n = 3$ ). These data validate the determination of relative TG accumulation based on the spectrophotometric absorbance of cell monolayers stained for neutral lipids with Oil Red O. Furthermore, TG accumulation found in AA-treated 3T3-L1 cells seems to be cell specific, as it was never observed in two other cell lines, myoblasts (C2C12) and hepatoma cells (HepG2), incubated with AA (data not shown).

To search for a potential role of ATP in TG accumulation induced by mitochondrial impairment in 3T3-L1 cells, we next tested the effect of AA, FCCP, and the adipogenic cocktail on cellular ATP content and found that all of these conditions led to a decrease (30–40% after 72 h) in ATP content (data not shown). However, as FCCP does not induce TG accumulation, energetic status by itself cannot explain the appearance of the multivesicular phenotype in AA-treated cells.

These results show that several inhibitors of mitochondrial oxidative phosphorylation, such as AA, rotenone, stigmatellin, myxothiazol, and oligomycin, induce TG accumulation in 3T3-L1 cells in a time- and concentration-dependent manner.

### Classical markers of differentiation are not observed in AA-treated 3T3-L1 cells

To further characterize the cell phenotype induced by AA, we looked for the abundance of FABP4/aP2, a molecular marker commonly used to monitor adipogenesis in vitro (Fig. 2A). We detected FABP4/aP2 during the whole differentiation program, with stronger expression after 7 and 8 days; FABP4/aP2 abundance remained low in cells incubated with AA. Other indices of adipocyte differentiation, such as the expression of C/EBP $\beta$  (Fig. 2B, C) or UCP-2 (Fig. 2D) and the transient increase in cell proliferation index (data not shown), were assessed in AA-treated 3T3-L1 cells, but none of these adipogenic features were upregulated in cells incubated with AA. Furthermore, cells incubated with the adipogenic cocktail in the presence of this inhibitor do not display adipogenic markers, as illustrated for C/EBP $\beta$  expression (Fig. 2B), and TG accumulation is reduced in these conditions (data not shown). Finally, TG accumulation induced by AA is still observed in 3T3-C2, a cell line that cannot differentiate in the presence of the adipogenic cocktail (18) (data not shown). Taken together, these results suggest that mechanisms involved in TG accumulation triggered by metabolic mitochondrial inhibitors are different from those leading to maturation of adipocytes in vitro.

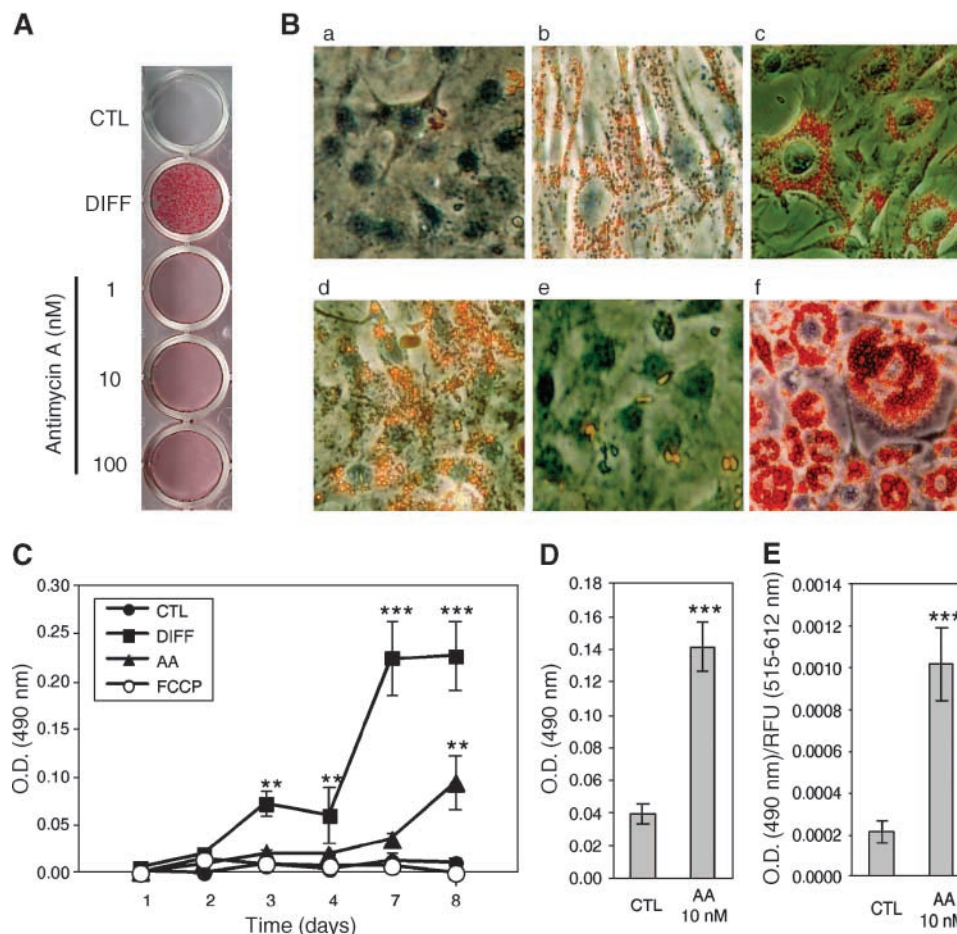


**Fig. 1.** Triglycerides (TGs) accumulate in 3T3-L1 cells treated with mitochondrial metabolic inhibitors targeting the electron transporter chain. **A:** Macroscopic visualization of neutral lipids stained with Oil Red O in control 3T3-L1 cells (CTL), cells incubated for 8 days with various concentrations of antimycin A (AA), or cells differentiated for 8 days with an adipogenic cocktail containing 1  $\mu$ M dexamethasone, 300  $\mu$ M dibutyryl cAMP, and 5  $\mu$ g/ml insulin (DIFF). **B:** Photomicrographs of 3T3-L1 cells treated or not (a) for 8 days with 10 nM AA (b), 100 nM stigmatellin (c), 8 nM oligomycin (d), or 1  $\mu$ M carbonyl cyanide (*p*-trifluoromethoxy)phenylhydrazone (FCCP; e) or for 8 days with an adipogenic cocktail (f) and stained for the presence of neutral lipids with Oil Red O. **C:** Quantitative determination of TG accumulation in 3T3-L1 cells incubated or not (CTL) for 1, 2, 3, 4, 7, or 8 days with the adipogenic cocktail (DIFF), 10 nM AA, or 1  $\mu$ M FCCP and stained with Oil Red O. The absorbance of cell monolayers was spectrophotometrically determined at 490 nm. **D, E:** Normalization of TG abundance for total DNA content. TGs in 3T3-L1 cells treated or not (CTL) for 8 days with 10 nM AA were stained with Oil Red O. Results were normalized (E) or not (D) for total DNA content, as determined by DNA labeling with fluorescent propidium iodide. Results are expressed as the absorbance of stained cell monolayers with Oil Red O at 490 nm (C, D) or as the absorbance normalized for relative fluorescence units (RFU; E) (means  $\pm$  SD;  $n = 3$  for C,  $n = 4$  for D, E). \*\* and \*\*\* Significantly different from corresponding control cells at  $P < 0.01$  and  $P < 0.001$ , respectively. O.D., optical density.

### Fatty acid $\beta$ -oxidation and steady-state mRNA level for M-CPT-1 are reduced in AA-treated cells

To better delineate the metabolic origin of TGs that accumulate during mitochondrial impairment, we first measured the uptake of TG precursors. Fatty acid and glycerol import were estimated by [ $^{14}$ C]oleate and [ $^3$ H]glycerol uptake assays, respectively. We found that differentiating cells increase the uptake of both precursors after 3 or 4 days of incubation (Fig. 3A, B). However, neither AA nor FCCP was able to induce the import of these molecules. We next performed fatty acid  $\beta$ -oxidation assays in 3T3-L1 cells incubated for 8 days with AA, FCCP, or the differentiation inducers. The  $\beta$ -oxidation rate was estimated by the

determination of filter-trapped  $^{14}\text{CO}_2$  released after the  $\beta$ -oxidation of preimported [ $^{14}$ C]oleate (Fig. 4A). We observed a decrease in fatty acid  $\beta$ -oxidation in both differentiated and AA-treated cells (40% and 70% reduction, respectively), whereas FCCP increased  $^{14}\text{CO}_2$  release (2-fold). These effects were still observed in the presence of AICAR, a well-known activator of AMPK and fatty acid  $\beta$ -oxidation (19).

CPT-1 is an enzyme that catalyzes the rate-limiting step of mitochondrial fatty acid  $\beta$ -oxidation (20). Therefore, we next analyzed the relative abundance of transcripts for the muscle isoform of CPT-1 (M-CPT-1) by real-time PCR (Fig. 4B). For three independent experiments, we found

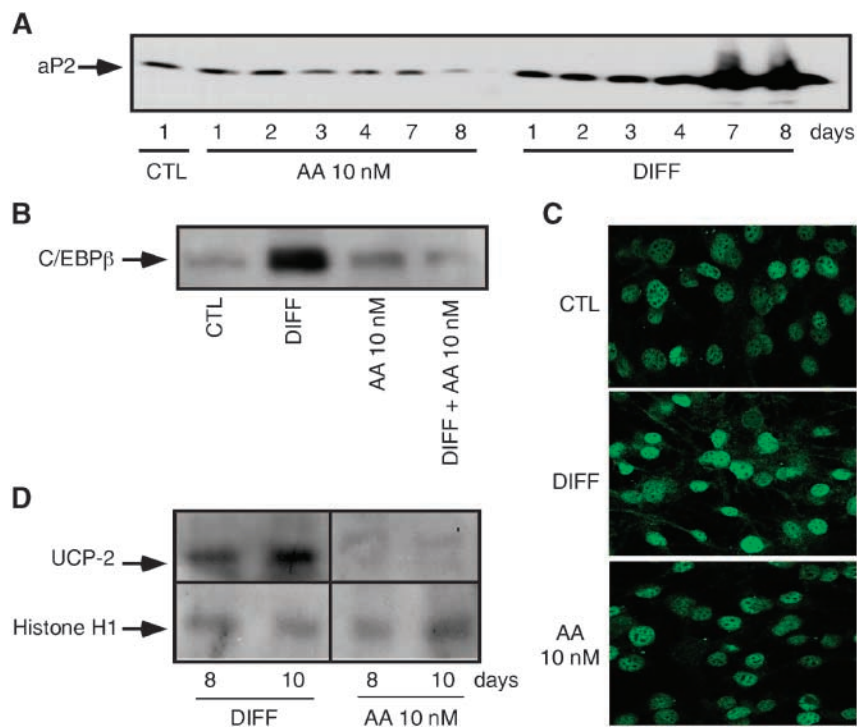


**Fig. 2.** AA does not induce adipocyte markers. **A:** Abundance of fatty acid binding protein 4 (FABP4)/aP2 determined by Western blot analysis performed on 20  $\mu$ g of lysate proteins prepared at the indicated times from 3T3-L1 cells incubated or not (CTL) with 10 nM AA or the adipogenic cocktail (DIFF). **B:** Abundance of CCAAT/enhancer binding protein  $\beta$  (C/EBP $\beta$ ) determined by Western blot analysis performed on 20  $\mu$ g of lysate proteins prepared from 3T3-L1 cells incubated or not (CTL) for 48 h with 10 nM AA, the adipogenic cocktail (DIFF), or combined conditions. **C:** Immunostaining and confocal microscopy analysis of the abundance and localization of C/EBP $\beta$  in 3T3-L1 cells incubated or not (CTL) for 48 h with 10 nM AA or with the adipogenic cocktail (DIFF). **D:** Western blot analysis for uncoupling protein-2 (UCP-2) performed on 20  $\mu$ g of lysate proteins prepared from 3T3-L1 cells incubated for 8 or 10 days with the adipogenic cocktail (DIFF) or with 10 nM AA. Equal protein loading was controlled by the immunodetection of histone H1.

that M-CPT-1 gene expression is downregulated in AA-treated cells compared with control cells ( $0.54 \pm 0.13$ ;  $P < 0.05$ ). Therefore, AA treatment decreases the abundance of the transcript for the M-CPT-1 isoform, whereas the expression of the liver isoform is unchanged ( $1.03 \pm 0.19$ ; data not shown). Expression of the M-CPT-1 gene also seems to be regulated in 3T3-L1 cells by PPAR $\gamma$  and its heterodimeric partner, RXR $\alpha$ , because in the presence of their respective ligands (ciglitazone and 9-*cis*-retinoic acid) the expression of M-CPT-1 is upregulated (2.6-fold increase).

Finally, the presence of AA completely inhibits the ligand-induced expression of M-CPT-1 (Fig. 4B). A PPAR $\gamma$ -dependent decrease in M-CPT-1 expression induced by AA thus could be a possible explanation for the decrease in  $\beta$ -oxidation observed in cells incubated with the mitochondrial inhibitor (Fig. 4A). To test this hypothesis, we next investigated the activity status of PPAR $\gamma$  in differentiating and AA-treated 3T3-L1 cells.

#### AA reduces PPAR $\gamma$ transcriptional activity

PPAR $\gamma$  is a well-known factor that controls lipid metabolism and the differentiation of preadipocytes (21). As this factor has been reported to be involved in the regulation of liver and M-CPT-1 expression (22), we measured the

binding activity of PPAR $\gamma$  to a synthetic DNA consensus sequence on nuclear proteins prepared from 3T3-L1 cells. The amount of PPAR $\gamma$  bound to a DR-1-containing oligonucleotide was determined with a colorimetric assay system. As expected, the amount of PPAR $\gamma$  that binds to DNA is rapidly increased in cells incubated with the adipogenic cocktail and remains high during the whole program (Fig. 5A). However, PPAR $\gamma$  DNA binding is not increased in AA-treated cells. As it has been reported that hypoxia antagonizes the transcription of the M-CPT-1 gene in cardiomyocytes through the inactivation of PPAR $\alpha$  (23), we next tested the effect of AA on PPAR $\gamma$  DNA binding activity induced by the differentiation cocktail. In these conditions, PPAR $\gamma$  DNA binding induced by the adipogenic cocktail is completely prevented in AA-treated cells (Fig. 5A). These results suggest that an inhibition of mitochondrial activity possibly could impair PPAR $\gamma$  binding to its consensus DNA sequence.

PPAR $\gamma$  acts as a heterodimer and is mainly associated with RXR $\alpha$  (24). Using the same colorimetric assay, we looked for a potential interaction between these two proteins using an anti-RXR $\alpha$  antibody to detect the bound heterodimer. We found that RXR $\alpha$  is part of the complex, as the detection profile obtained for this factor is similar to the binding pattern observed for PPAR $\gamma$  (Fig. 5B). This



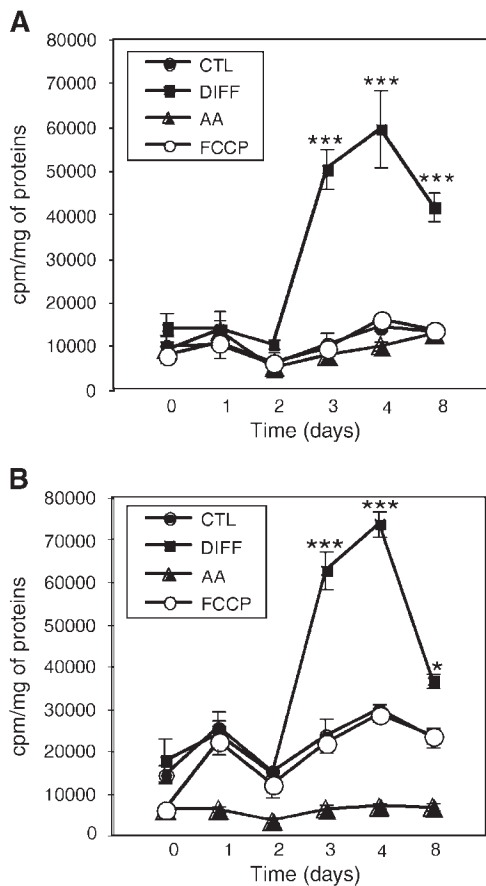


**Fig. 3.** TG precursor uptake is increased in differentiating 3T3-L1 cells but not in AA-treated cells. Oleate and glycerol uptake assays performed on 3T3-L1 cells incubated or not (CTL) with the adipogenic cocktail (DIFF), with 10 nM AA, or with 1  $\mu$ M FCCP. After 5 h (day 0) or several days of treatment, cells were incubated for 90 min with 1  $\mu$ Ci/ml [ $^{14}$ C]oleate (A) and 1  $\mu$ Ci/ml [ $^3$ H]glycerol (B) before the radioactivity associated with cell monolayers was counted. Results are expressed in cpm/mg of proteins (means  $\pm$  SD;  $n = 3$ ). \* and \*\*\* Significantly different from corresponding control cells at  $P < 0.05$  and  $P < 0.001$ , respectively.

result suggests that both proteins interact physically when bound to the DR-1 consensus sequence. In samples prepared from cells incubated with AA or with the adipogenic cocktail in the presence of the mitochondrial inhibitor, the signal for RXR $\alpha$  bound to PPAR $\gamma$  is not increased.

Furthermore, the adipogenic cocktail triggers the activity of PPAR $\gamma$ , as demonstrated in cells transiently transfected with a luciferase reporter construct sensitive to PPAR $\gamma$  (Fig. 5C). The luciferase activity measured in differentiating cells is comparable to the activity measured in cells that overexpress PPAR $\gamma$ 2. On the other hand, AA is unable to trigger the activation of the PPAR $\gamma$ -sensitive reporter construct (Fig. 5D). We found that the PPAR $\gamma$ -dependent transactivation of the reporter gene induced by ciglitazone and 9-*cis*-retinoic acid is dramatically inhibited in cells that are coinubated with the mitochondrial metabolic inhibitor. This effect is even better visualized in cells that overexpress PPAR $\gamma$ 2 (Fig. 5D). We finally checked the abundance of PPAR $\gamma$  in the nuclei of 3T3-L1 cells in-

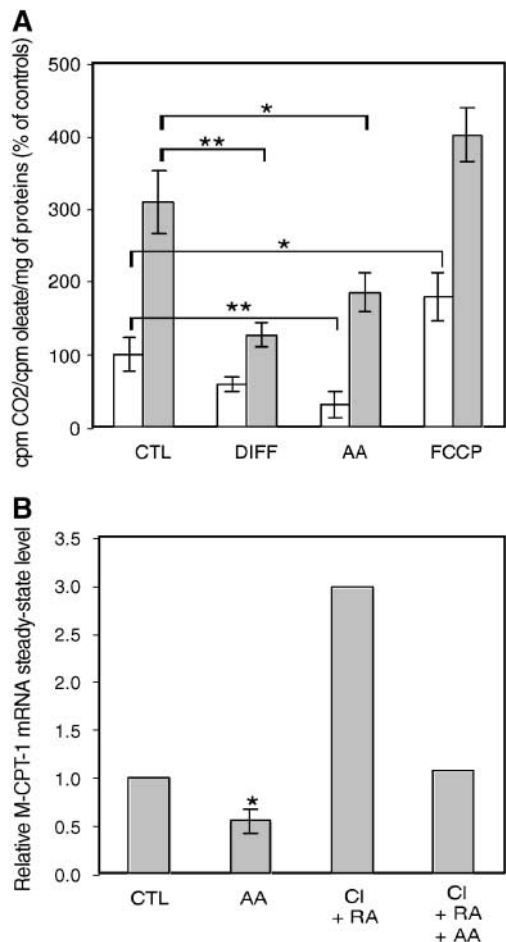


**Fig. 4.** Fatty acid  $\beta$ -oxidation and muscle carnitine palmitoyl transferase-1 (M-CPT-1) expression are decreased in AA-treated 3T3-L1 cells. A: Determination of fatty acid  $\beta$ -oxidation rate in 3T3-L1 cells incubated with the adipogenic cocktail (DIFF), with 10 nM AA, or with 1  $\mu$ M FCCP. After 8 days of treatment, cells were preincubated (gray bars) or not (white bars) with 500  $\mu$ M 5-aminoimidazole-4-carboxamide-1- $\beta$ -D-ribofuranoside (AICAR) for 180 min and then incubated for 90 min in the presence of 1  $\mu$ Ci/ml [ $^{14}$ C]oleate with (gray bars) or without (white bars) 500  $\mu$ M AICAR. Released  $^{14}$ CO<sub>2</sub> was harvested on filter papers and subjected to radioactivity counting. Results are expressed in cpm  $^{14}$ CO<sub>2</sub> normalized for the cpm of the [ $^{14}$ C]oleate taken up and for protein content and are presented as percentages of controls (means  $\pm$  SD;  $n = 3$ ). B: Effect of AA and peroxisome proliferator-activated receptor  $\gamma$ /retinoid X receptor  $\alpha$  (PPAR $\gamma$ /RXR $\alpha$ ) activators on M-CPT-1 mRNA steady-state levels determined by real-time PCR. 3T3-L1 cells were incubated for 8 days with 10 nM AA, 10  $\mu$ M ciglitazone (CI), or 10  $\mu$ M 9-*cis*-retinoic acid (RA) or with a combination of these three molecules before mRNA was extracted and reverse-transcribed. Quantitative real-time PCR with specific primers for M-CPT-1 transcripts was performed. TATA box binding protein (TBP)/TFIID was used for normalization. Results are expressed as relative mRNA steady-state level compared with control cells (CTL) for  $n = 3$  (CTL and AA-treated cells) or  $n = 2$  (CI+RA- and CI+RA+AA-treated cells). \* and \*\* Significantly different from corresponding control cells at  $P < 0.05$  and  $P < 0.01$ , respectively.

incubated with AA by Western blot analysis performed on nuclear proteins. In these conditions, we found a strong decrease in the nuclear abundance of PPAR $\gamma$  in cells preincubated with AA (Fig. 5E). Altogether, these results clearly

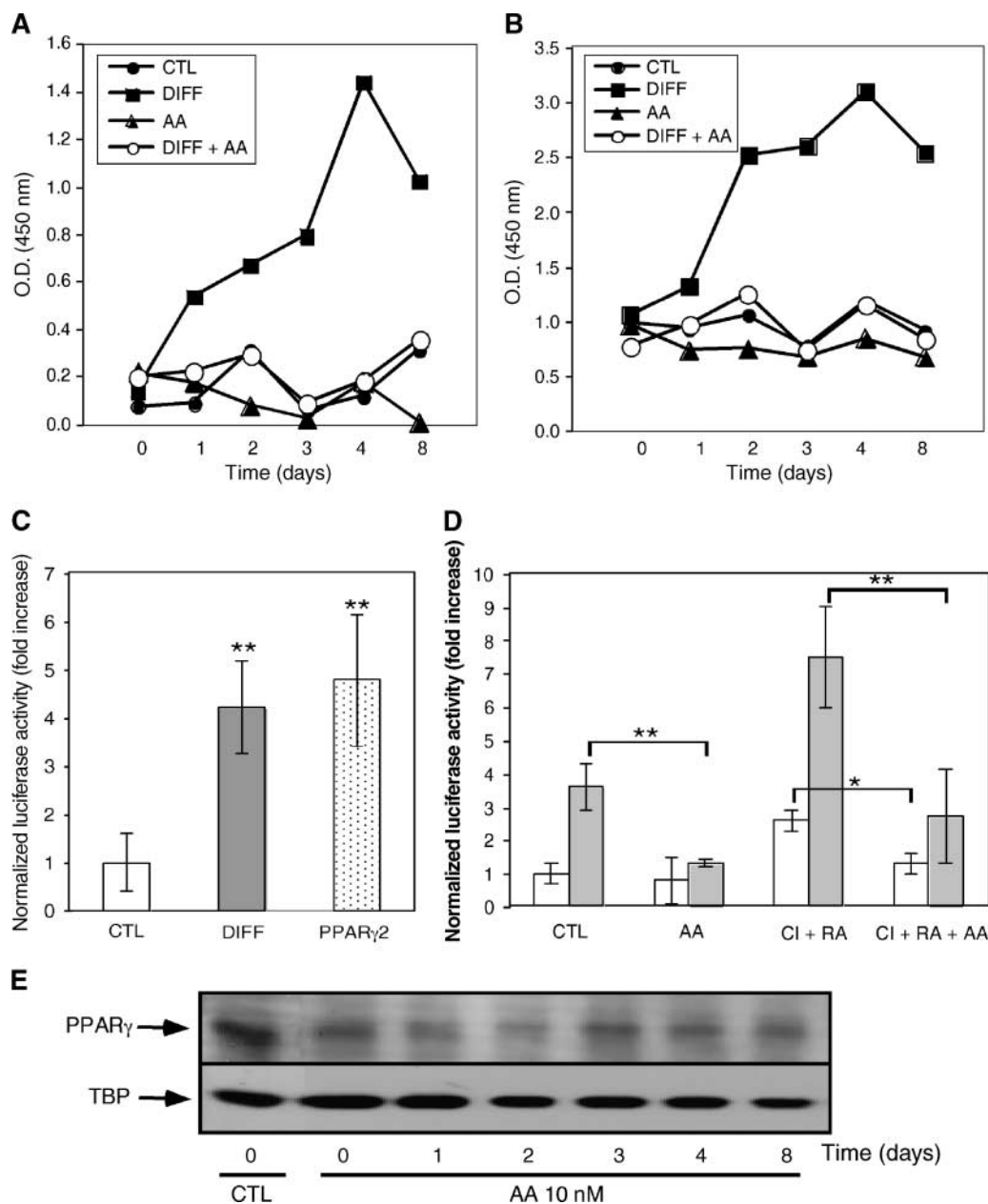


**Fig. 5.** AA decreases PPAR $\gamma$  activity. A, B: PPAR $\gamma$  (A) and RXR $\alpha$  (B) DNA binding colorimetric assays (TransAM kit) performed with 5  $\mu$ g of nuclear proteins extracted from 3T3-L1 cells incubated or not (CTL) for 6 h (day 0) or several days with the adipogenic cocktail (DIFF), 10 nM AA, or a combination of both. Protein binding to DNA was detected with an anti-PPAR $\gamma$  or anti-RXR $\alpha$  antibody. Results are expressed as mean optical density (O.D.) values at 450 nm ( $n = 2$ ). C: PPAR $\gamma$ -dependent activity in differentiating 3T3-L1 cells. Cells were transiently cotransfected with a  $\beta$ -galactosidase expression vector and a PPAR $\gamma$ -sensitive luciferase reporter construct (tk-PPREx3-Luc), with a PPAR $\gamma$ 2 expression vector (PPAR $\gamma$ 2), or PGL2 plasmid (CTL, DIFF). Directly after transfection, cells were incubated (DIFF) or not (CTL, PPAR $\gamma$ 2) for 48 h with the adipogenic cocktail and then processed for luciferase assay. D: Effect of AA on PPAR $\gamma$  activity in 3T3-L1 cells cotransfected with a  $\beta$ -galactosidase expression vector and the tk-PPREx3-Luc reporter construct, with a PPAR $\gamma$ 2 expression vector (gray bars), or PGL2 vector (white bars). After transfection, cells were incubated or not (CTL) for 48 h with 10 nM AA, with 10  $\mu$ M 9-*cis*-retinoic acid and 10  $\mu$ M ciglitazone (RA+CI), or with a combination of these three molecules (RA+CI+AA) before luciferase assay. Results are normalized for  $\beta$ -galactosidase activity and are expressed as fold increases of control cells [means  $\pm$  SD for  $n = 4$  (C) or  $n = 3$  (D)]. \* and \*\* Significantly different from corresponding control cells at  $P < 0.05$  and  $P < 0.01$ , respectively. E: Nuclear abundance of PPAR $\gamma$  in AA-treated 3T3-L1 cells determined by Western blot analysis performed on 20  $\mu$ g of nuclear proteins extracted after 5 h (day 0) or 1, 2, 3, 4, or 8 days of incubation. Equal protein loading was checked by the immunodetection of TBP.



show that the transcriptional activity of PPAR $\gamma$  is inhibited in 3T3-L1 cells when mitochondrial activity is impaired.

### AA induces GLUT4 translocation and glucose uptake by a calcium- and a PI 3-kinase-dependent mechanism

Acute stimulation of glucose transport in response to hypoxia and inhibition of oxidative phosphorylation represent an important homeostatic mechanism because it enables the stimulation of ATP formation by glycolysis (25). However, glucose might have another role in cells with impaired mitochondrial activity, as some derivatives, such as xylulose 5-phosphate, can activate the transcription factor ChREBP (26). We thus studied the contribution of glucose to the accumulation of TG in 3T3-L1 cells incubated with AA. We first used 2-deoxy- $^{3}\text{H}$ glucose (2-DG) uptake assays to test the effect of the adipogenic cocktail, AA, and FCCP on glucose uptake. As shown in Fig. 6A, we observed that after 48 h of incubation, AA significantly stimulates glucose uptake. A kinetic study has shown that glucose uptake is rapidly (within 6 h) induced by the inhibition of mitochondrial activity. The 2-DG uptake in these

conditions is specific and involves GLUTs, as it is completely inhibited in the presence of 40 nM cytochalasin B (Fig. 6A). To identify the GLUT involved in glucose uptake, we next analyzed the abundance of the insulin-responsive GLUT4 by Western blotting performed on purified plasma membranes prepared from 3T3-L1 cells incubated or not for 48 h with AA (Fig. 6B). We observed that GLUT4 is strongly translocated to the plasma membrane of AA-incubated 3T3-L1 cells. Furthermore, glucose uptake by cells incubated in the presence of the mitochondrial inhibitor is completely abolished in the presence of 20  $\mu\text{M}$  cytochalasin D (data not shown), a drug that inhibits globular actin polymerization into filamentous actin and prevents insulin-dependent recruitment of GLUTs such as GLUT4 to the plasma membrane (27).

GLUT4 translocation to plasma membrane and activity can be regulated by several mechanisms and kinases, such as PI 3-kinase and AMPK, depending mainly on cell type and stimuli (28). To identify messengers and kinases activated by mitochondrial inhibition that could stimulate glucose uptake, we investigated the effect of BAPTA-AM

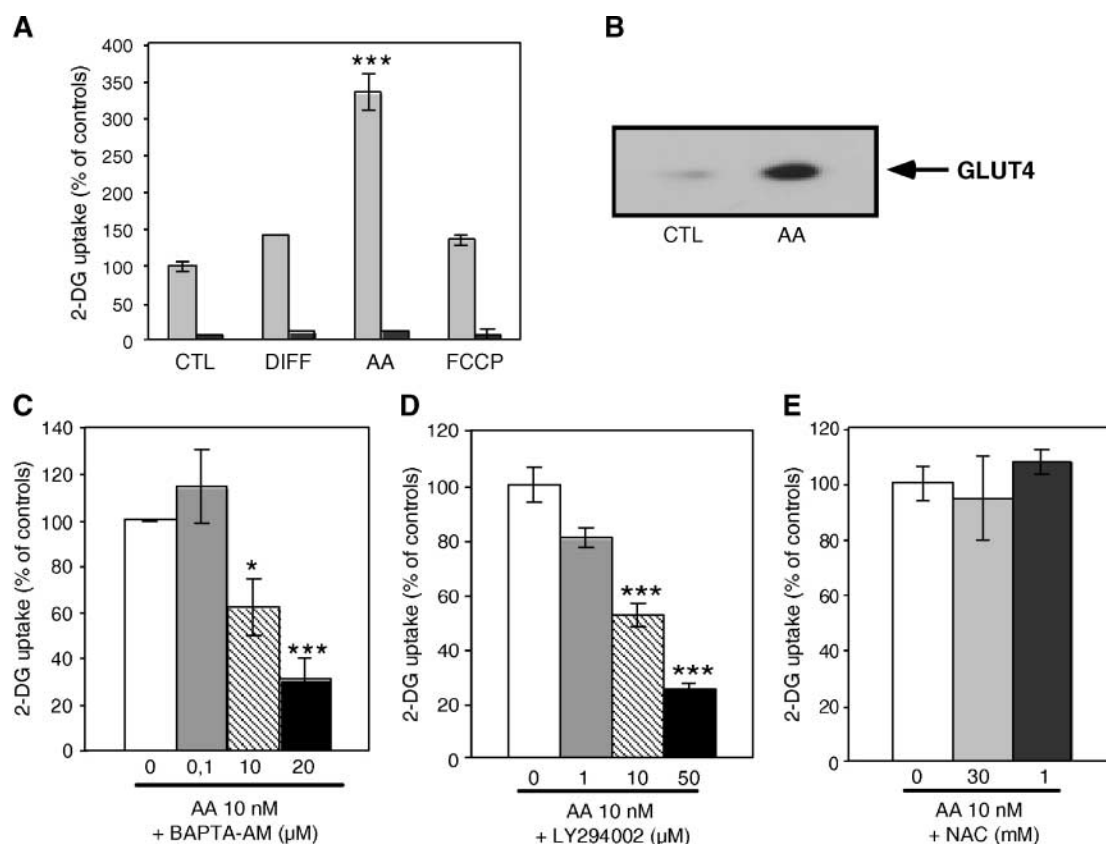


**Fig. 6.** AA induces glucose transporter 4 (GLUT4) translocation and glucose uptake by a calcium- and phosphatidylinositol 3-kinase (PI 3-kinase)-dependent mechanism. A: Glucose uptake assay was performed on 3T3-L1 cells incubated or not (CTL) with the adipogenic cocktail (DIFF), 10 nM AA, or 1  $\mu\text{M}$  FCCP. After 48 h of treatment, cells were preincubated (black) or not (gray) for 4 h with 40 nM cytochalasin B and then incubated for 30 min with 1  $\mu\text{Ci}/\text{ml}$  2-deoxy-D- $^{3}\text{H}$ glucose (2-DG) before the cell-associated radioactivity was counted. B: Western blot analysis of GLUT4 abundance in crude plasma membranes prepared from 3T3-L1 cells incubated or not (CTL) with 10 nM AA for 48 h. C–E: Glucose uptake by 3T3-L1 cells treated for 48 h with 10 nM AA, preincubated for 3 h with or without 1,2-bis(2-aminophenoxy)ethane-*N,N,N',N'*-tetraacetic acid (BAPTA-AM; C), LY294002 (D), or *N*-acetyl-L-cysteine (NAC; E), and then incubated for 30 min in the presence of 1  $\mu\text{Ci}/\text{ml}$  2-DG containing or not BAPTA-AM, LY294002, or NAC at the same concentration. Radioactivity was counted on cell lysates and normalized for protein amounts. Results are expressed as percentages of the corresponding control (means  $\pm$  SD;  $n = 3$ ). \* and \*\*\* Significantly different from control cells at  $P < 0.05$  and  $P < 0.001$ , respectively.

(an intracellular calcium chelator), LY294002 (a PI 3-kinase inhibitor), and NAC (an antioxidant molecule) on 2-DG uptake induced by a 48 h treatment with AA (Fig. 6C–E). BAPTA-AM and LY294002 both inhibit 2-DG uptake in a concentration-dependent manner, suggesting a role for calcium and PI 3-kinase pathways in AA-induced glucose uptake, whereas NAC has no effect. The role of the PI 3-kinase pathway is also supported by the fact that the abundance

of p110 $\alpha$  (the catalytic subunit of PI 3-kinase) is strongly increased in cells incubated with AA for 48 h (Fig. 7A).

As an upstream marker of PI 3-kinase activation, we next looked for the phosphorylation status of insulin receptor substrate-1 (IRS-1) on Tyr941, an adaptor molecule recruiting the regulatory subunit of PI-3 kinase (p85) after insulin receptor activation, and found that AA triggers the phosphorylation of IRS-1 (data not shown). Further-

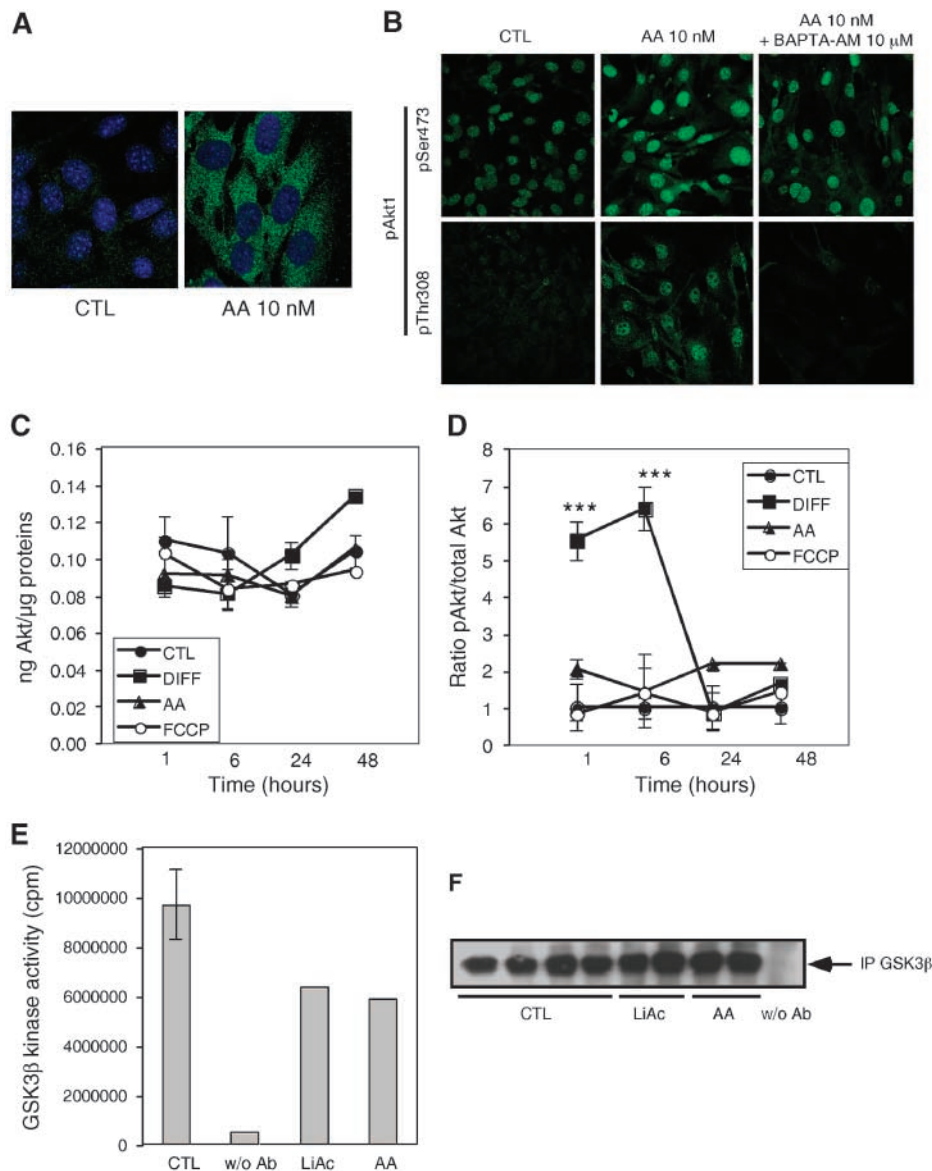


**Fig. 7.** AA activates the PI 3-kinase/Akt1/glycogen synthase kinase 3 $\beta$  (GSK3 $\beta$ ) pathway. A: Immunofluorescence staining and confocal microscopy visualization of p110 $\alpha$  performed on 3T3-L1 cells incubated for 48 h with or without (CTL) 10 nM AA. Nuclei were visualized with ToPro-3. B: Immunofluorescence staining and confocal microscopy visualization of pSer473-Akt1 and pThr308-Akt1 performed on 3T3-L1 cells treated for 48 h with or without (CTL) 10 nM AA and preincubated or not for 2 h in the presence of 10  $\mu$ M BAPTA-AM. C, D: Total Akt1 (C) and pSer473-Akt1 (D) ELISAs performed on 10  $\mu$ g of lysate proteins prepared from 3T3-L1 cells incubated or not (CTL) with the adipogenic cocktail (DIFF), 10 nM AA, or 1  $\mu$ M FCCP for the indicated times. Results for total Akt1 are expressed in ng/ $\mu$ g proteins. Data for pAkt1 are normalized for total Akt1 amount and are expressed as fold increases of control cells (means  $\pm$  SD; n = 3). \*\*\* Significantly different from control cells at  $P < 0.001$ . E: In vitro kinase activity of immunoprecipitated GSK3 $\beta$  from 3T3-L1 cells incubated or not (CTL) for 48 h with 10 nM AA. In some conditions, lithium acetate (LiAc) at 40  $\mu$ M was added as a control for specificity. w/o Ab, without antibody. F: Western blot analysis of immunoprecipitated GSK3 $\beta$ .

more, Akt1 phosphorylation on both Ser473 (Fig. 7B–D) and Thr308 (Fig. 7B) residues is increased in 3T3-L1 cells incubated in the presence of the mitochondrial metabolic inhibitor for 48 h. As expected, Akt1 is rapidly and transiently phosphorylated on Ser473 in the presence of the adipogenic cocktail (Fig. 7D). More interestingly, we observed that AA-induced Akt1 phosphorylation on Thr308 is totally inhibited in the presence of BAPTA-AM (Fig. 7B), suggesting a role for calcium in the full activation of Akt1 by AA. We also observed that Akt1 localization is mainly nuclear in all conditions (Fig. 7B), an observation already reported by others (29).

Finally, the *in vitro* kinase activity of immunoprecipitated GSK3 $\beta$ , a PI 3-kinase pathway effector that can be inhibited by an Akt-dependent phosphorylation on Ser9 (30), was determined (Fig. 7E, F). In cells incubated with 10 nM AA for 48 h, the activity of GSK3 $\beta$  is reduced by 40%. This inhibition is comparable to the effect obtained when lithium, a GSK3 $\beta$  inhibitor (31), is added during the kinase assay. The role of GSK3 $\beta$  inhibition in glucose uptake by 3T3-L1 cells was then determined using SB216763, a specific inhibitor of GSK3 $\beta$  (Fig. 8). We observed that SB216763 induces a significant increase in basal glucose uptake by control cells, suggesting that GSK3 $\beta$  inhibition is one of the mechanisms involved in glucose uptake in 3T3-L1 preadipocytes. However, SB216763 did not stimulate further glucose uptake by cells incubated with AA. These results suggest that the inhibition of GSK3 $\beta$  in cells incubated with the mitochondrial inhibitor could be a possible mechanism by which glucose uptake is stimulated in 3T3-L1 cells in these conditions.

AMPK is another serine/threonine kinase known to regulate glucose uptake mainly in muscle cells (32). By immunostaining, and as expected for this “energetic sensor,” we observed that AMPK is transiently phosphorylated

on Thr172 in cells incubated for 24 h with AA (Fig. 9A). AMPK activation was confirmed by the fact that AA also triggers the phosphorylation of ACC on Ser79, a well-known AMPK substrate, to a similar level than phosphorylation obtained for a short cell stimulation with AICAR (Fig. 9B). However, AMPK does not seem to be involved in the AA-induced glucose uptake by 3T3-L1 cells, as neither AICAR nor the overexpression of a dominant negative form of AMPK (33) significantly alters glucose uptake by control cells or cells incubated with AA for 48 h (Fig. 9C, D).

#### TG storage in 3T3-L1 cells incubated with AA is inhibited by BAPTA-AM, LY294002, and cytochalasin B

It is interesting that molecules that inhibit AA-induced glucose uptake, such as cytochalasin B, BAPTA-AM, and LY294002 (Fig. 6A, C, D), are also able to significantly reduce the amount of TG that accumulates in cells incubated with the mitochondrial inhibitor for 8 days (Fig. 10). These results allow us to hypothesize that glucose, massively taken up by AA-incubated preadipocytes, contributes to TG accumulation.

#### Dual role for glucose in TG accumulation in preadipocytes incubated with AA

To further delineate the contribution of glucose to the accumulation of TG observed in preadipocytes with a mitochondrial dysfunction, we first measured glucose conversion into TG by recovering the radioactivity associated with extracted neutral lipids from cells preincubated with AA or the adipogenic cocktail for 8 days and then incubated briefly with radiolabeled D- $^{14}\text{C}$ (U)glucose (Fig. 11A). In these conditions, we found that the radioactivity associated with TG is significantly increased in AA-treated cells, whereas the adipogenic cocktail does not induce  $^{14}\text{C}$  incorporation into lipids. Taken together, these results suggest a glucose-to-TG conversion in 3T3-L1 cells incubated with AA.

Finally, as ChREBP is a transcription factor known to regulate the expression of glycolytic and lipogenic genes (26), we transiently transfected 3T3-L1 cells with a luciferase reporter construct responsive to this factor. AA consistently triggered a 2- to 3-fold activation of the ChREBP-sensitive reporter gene in cells incubated for 24 h with the mitochondrial inhibitor (Fig. 11B). These results clearly indicate that glucose taken up by AA-treated cells can activate a transcription factor known to control the expression of genes involved in glycolysis and lipogenesis, such as L-PK, FAS, and ACC. The potential contribution of lipogenesis in AA-induced TG vesicle formation is also supported by the fact that EGCG, an inhibitor of ACC that catalyzes the first reaction of fatty acid synthesis, completely inhibits TG accumulation in cells incubated with AA (Fig. 11C).

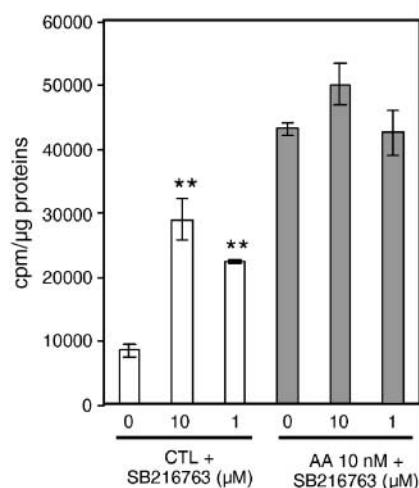


**Fig. 8.** Effect of the GSK3 $\beta$  inhibitor SB216763 on glucose uptake in 3T3-L1 cells. Cells were incubated or not (CTL) for 48 h with 10 nM AA. Cells were then preincubated or not for 2 h with SB216763 before a glucose uptake assay was performed. Results are expressed as cpm normalized for protein content (means  $\pm$  SD;  $n = 3$ ). \*\* Significantly different from control cells at  $P < 0.01$ .

## DISCUSSION

Mitochondrial deficiency can regulate nuclear gene expression by a process called mitochondria-nucleus retrograde communication, which allows cells to differentially express some mitochondrial target genes by changing the



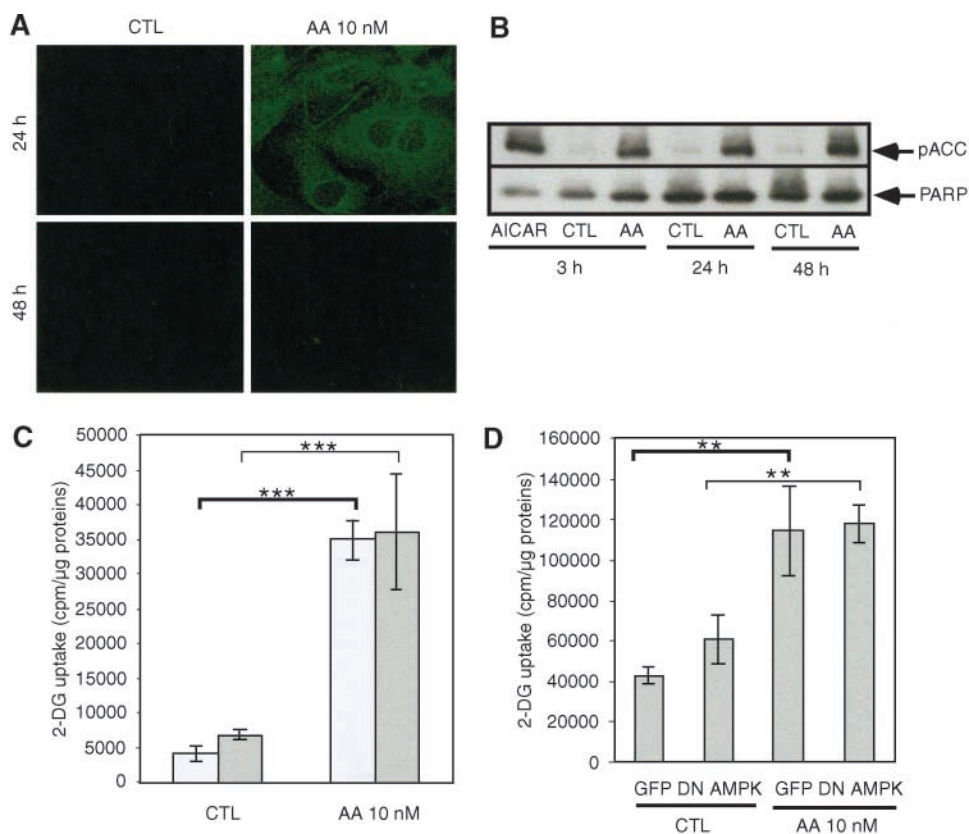


**Fig. 9.** AMP-dependent kinase (AMPK) is rapidly and transiently activated by AA but is not involved in AA-induced glucose uptake. **A:** Immunofluorescence staining and confocal microscopy visualization of pThr172-AMPK performed on 3T3-L1 cells incubated or not (CTL) with 10 nM AA for 24 or 48 h. **B:** Abundance of Ser79-phosphorylated acetyl-coenzyme A carboxylase (ACC) determined by Western blot analysis performed on 20 μg of lysate protein prepared from 3T3-L1 cells incubated or not (CTL) for 3 h with 500 μM AICAR or for 3, 24, or 48 h with 10 nM AA. Equal protein loading was checked by the immunodetection of poly-ADP ribose protein (PARP). **C:** Glucose uptake assay performed on 3T3-L1 cells treated for 48 h with 10 nM AA, preincubated for 3 h with (gray bars) or without (white bars) 500 μM AICAR, and then incubated for 30 min with 1 μCi/ml 2-DG containing AICAR or not before radioactivity was counted on cell lysates. RLU, relative light units. **D:** Effect of the overexpression of a dominant negative form of AMPK (DN AMPK) in 3T3-L1 cells on glucose uptake. Cells were transiently transfected by electroporation with 5 μg of a green fluorescent protein (GFP) expression vector or with the dominant negative form of AMPK. Cells were then incubated or not (CTL) with 10 nM AA for 48 h before the glucose uptake assay. Results are expressed as cpm/μg proteins (means ± SD; n = 3). \*\* and \*\*\* Significantly different from corresponding control cells at  $P < 0.01$  and  $P < 0.001$ , respectively.

activity of some transcription factors (34), a phenomenon initially observed in yeast (35) and more recently in mammalian cells (11, 36). Here, we studied the response of 3T3-L1 preadipocytes to mitochondrial dysfunction, a condition that has previously been associated with an atypical adipocyte phenotype (7) observed in pathologies characterized by dyslipidemia or lipodystrophy (2). To address the mechanisms by which mitochondrial dysfunction can lead to an increase in cytosolic TG content, 3T3-L1 preadipocytes were subjected to a prolonged mitochondrial activity inhibition induced by inhibitors of oxidative phosphorylation. We showed that rotenone, AA, stigmatellin, myxothiazol, and oligomycin induce an accumulation of intracellular TG vesicles. However, the multivesicular phenotype observed in these conditions is different from the phenotype obtained for adipocytes differentiated *in vitro*. Interestingly, the adipogenic cocktail and all mitochon-

drial inhibitors tested, including the uncoupler FCCP, reduce cellular ATP content. However, FCCP does not trigger TG vesicle formation, suggesting that cytosolic lipid accumulation is not a direct consequence of ATP decline. The mechanisms leading to TG storage in 3T3-L1 cells treated with AA also seem to be different from those leading to adipocyte differentiation, as AA-triggered TG accumulation observed in 3T3-L1 cells still occurs in 3T3-C2 cells, a close but nondifferentiable cell line, with the adipogenic cocktail (18). Moreover, the inhibition of mitochondrial respiration does not induce the expression of classical adipogenic markers, such as FABP4/aP2, C/EBPβ, PPARγ, and UCP-2. TG accumulation in response to mitochondrial inhibition also appears to be cell-specific, as it was not observed in C2C12 myoblasts or in HepG2 hepatoma cells in our experimental conditions. However, TG accumulation has already been described in cardiac myocytes

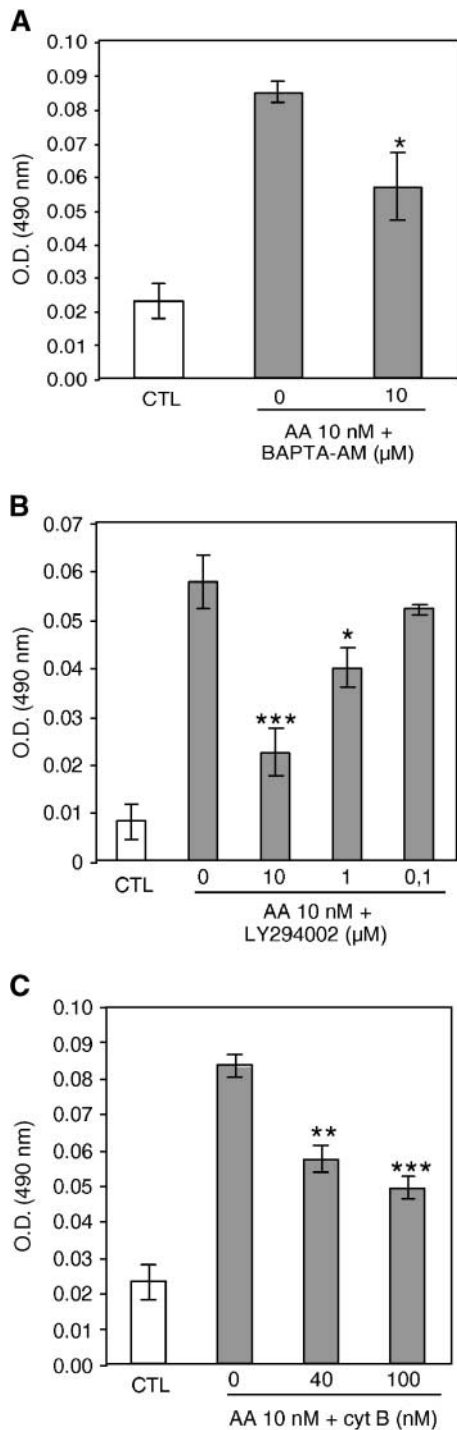


**Fig. 10.** AA-induced TG accumulation is mediated by calcium and PI-3 kinase and is dependent on glucose uptake. Cells were incubated or not (CTL) with 10 nM AA in the presence or not of BAPTA-AM (A), LY294002 (B), or cytochalasin B (cyt B; C) at the indicated concentrations. After 8 days of incubation, TGs were stained with Oil Red O and absorbance was measured. Results are expressed as optical density (O.D.) values at 490 nm (means  $\pm$  SD;  $n = 3$ ). \*, \*\*, and \*\*\* Significantly different from corresponding control cells at  $P < 0.05$ ,  $P < 0.01$ , and  $P < 0.001$ , respectively.

incubated under hypoxia, a condition also known to impair mitochondrial respiration (23).

In this study, we provide strong evidence that both a reduction in fatty acid  $\beta$ -oxidation and glucose participate

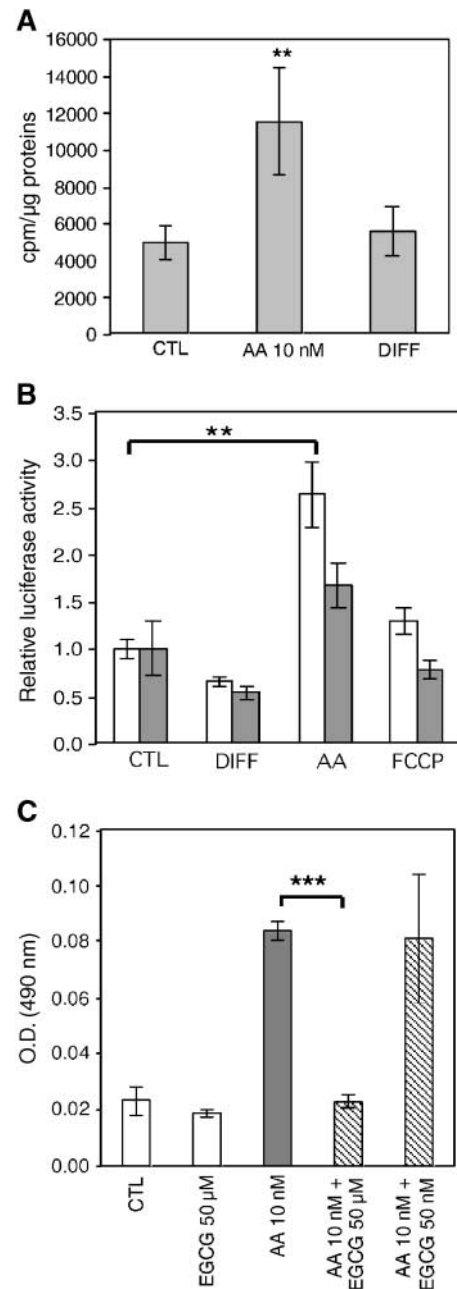


**Fig. 11.** AA increases glucose conversion into TGs and triggers the activation of carbohydrate-responsive element binding protein (ChREBP) in 3T3-L1 cells. A: Cells were incubated or not (CTL) for 8 days with 10 nM AA or the adipogenic cocktail (DIFF) and for 90 min in the presence of 5  $\mu$ M [ $^{14}$ C]glucose. Lipids were then extracted and TG-associated  $^{14}$ C radioactivity was counted. Results are expressed in cpm normalized for protein content (means  $\pm$  SD;  $n = 5$ ). B: ChREBP-dependent luciferase activity in 3T3-L1 cells transiently cotransfected with a ChREBP-sensitive luciferase reporter construct and a  $\beta$ -galactosidase expression vector. After a 16 h recovery, cells were incubated or not (CTL) for 24 h (white bars) or 48 h (gray bars) with the adipogenic cocktail (DIFF), 10 nM AA, or 1  $\mu$ M FCCP. Cells were then processed for luciferase assay. Results were normalized for  $\beta$ -galactosidase activity and are expressed as fold induction of the corresponding controls (means  $\pm$  SD;  $n = 3$ ). C: Oil Red O staining performed on 3T3-L1 cells incubated for 8 days with or without (white bars) 10 nM AA in the presence (hatched bars) or absence (gray bars) of (-)-epigallocatechin gallate (EGCG). Results are expressed in optical density (O.D.) values at 490 nm (means  $\pm$  SD;  $n = 3$ ). \*\* and \*\*\* Significantly different from control cells at  $P < 0.01$  and  $P < 0.001$ , respectively.

to TG accumulation in preadipocytes with impaired mitochondrial activity. First, we showed that the uptake of TG precursors is increased during adipogenesis but is unchanged in cells incubated with AA. Therefore, TG accumulation in 3T3-L1 cells with mitochondrial dysfunction is unlikely to result from a direct uptake of TG precursors. Moreover, the expression of FABP4/aP2, a PPAR $\gamma$ -regulated gene (37) encoding a protein involved in fatty acid intracellular transport and frequently used as a marker of adipocyte differentiation, remains very low in 3T3-L1 cells treated with AA. Consistent with this finding, we did not measure any PPAR $\gamma$  activation in preadipocytes treated with AA.

We also found a decrease in the fatty acid  $\beta$ -oxidation rate in cells treated with AA as well as in cells incubated with the differentiation inducers, an effect even more evident when cells are preincubated with AICAR before the  $\beta$ -oxidation assay. This AMP structural analog stimulates  $\beta$ -oxidation through AMPK-mediated ACC inhibition, leading to a decrease in malonyl-CoA concentration, resulting in an increase in CPT-1 activity (38), the enzyme that catalyzes the rate-limiting step in the mitochondrial import of fatty acids (20). We thus propose that this mechanism participates in AA-induced TG accumulation in preadipocytes. This hypothesis is supported by the fact that the expression of M-CPT-1, a PPAR target gene (37), is downregulated in 3T3-L1 cells incubated with the mitochondrial inhibitor. PPARs are key regulators involved in the differentiation of several cell types (39) and in fat metabolism (21, 40). We also found that AA is unable to stimulate the binding of the PPAR $\gamma$ /RXR $\alpha$  heterodimer to a consensus DNA sequence, whereas the adipogenic cocktail triggers PPAR $\gamma$ /RXR $\alpha$  DNA binding and activity, as described previously (41). Interestingly, the addition of AA to the cells at the same time as the adipogenic cocktail completely abolished PPAR $\gamma$  and RXR $\alpha$  DNA binding and the resulting C/EBP $\beta$  overexpression. Moreover, we found that in the presence of AA, PPAR $\gamma$ /RXR $\alpha$  transcriptional activity stimulated by ciglitazone and 9-*cis*-retinoic acid is reduced dramatically. These results show that the inhibitor of complex III antagonizes PPAR $\gamma$ /RXR $\alpha$ -dependent gene transcription in 3T3-L1 cells, probably through a decrease in PPAR $\gamma$  nuclear abundance, as suggested by Western blot analysis. As PPAR $\gamma$  also controls the expression of genes encoding enzymes involved in the mitochondrial  $\beta$ -oxidation cycle, such as the medium-chain acyl-CoA dehydrogenase (42), PPAR $\gamma$  inactivation could also inhibit  $\beta$ -oxidation through downregulation of gene expression other than M-CPT-1, such as medium-chain acyl-CoA dehydrogenase. We also found by real-time PCR that transcript abundance for liver CPT-1, the major CPT-1 isoform expressed in 3T3-L1 cells (43), is not affected by AA treatment, whereas M-CPT-1 is downregulated. These results are surprising, as both promoters can be activated by similar transcription factors such as PPARs (22) and both isoforms can be upregulated by the overexpression of PPAR $\gamma$  coactivator-1 (44). However, promoters of these genes contain several binding sites for other transcription factors, such as cAMP-response element binding protein, hepatic nuclear factor-4 $\alpha$ , and thyroid hormone receptor

(22, 45) as well as factors such as upstream stimulatory factor 1/2 (52). Furthermore, it has been reported that CPT-1 expression is switched from the liver to the muscle isoform during adipogenesis in several species (43). Thus, these data suggest a possible differential regulation of both isoforms, as observed in our experimental conditions.

Cytosolic fatty acid synthesis and mitochondrial  $\beta$ -oxidation are two pathways reciprocally regulated through the inhibitory effect of malonyl-CoA on CPT-1 activity (38). Here, we show that a decrease in fatty acid  $\beta$ -oxidation might be a major mechanism by which TGs accumulate inside preadipocytes when mitochondrial respiration is depressed by direct inhibition of the respiratory chain. However, one cannot completely rule out a contribution of active fatty acid synthesis in AA-treated 3T3-L1 cells, as ACC inhibition by EGCG added during AA treatment prevents TG accumulation. In the future, the metabolic partitioning of endogenous fatty acids and the balance among synthesis, oxidation, and TG hydrolysis, which determine the net quantity of cellular fat content, should be fully addressed in preadipocytes with impaired mitochondrial respiration.

Previous studies on cataplerosis showed the important role of glucose in lipogenesis in several cellular models (46). As 3T3-L1 cells treated with a mitochondrial inhibitor increase glucose uptake for their glycolytic needs, we studied the potential role of glucose in TG accumulation. In differentiated 3T3-L1 cells, NaN<sub>3</sub> and dinitrophenol increase basal glucose uptake mediated by GLUT1 and inhibit GLUT4-dependent insulin-induced glucose transport (47). Even if we cannot rule out the participation of GLUT1 activation in AA-induced glucose uptake (48), we show that GLUT4 abundance is increased in plasma membrane of 3T3-L1 cells incubated with AA, suggesting that GLUT4 translocation from cytosolic storage vesicles is induced by this mitochondrial inhibitor, as observed previously in L6 cells with impaired mitochondria (49). We also demonstrated that glucose uptake and TG accumulation triggered by AA can both be inhibited by a PI 3-kinase inhibitor (LY294002) and a calcium chelator (BAPTA-AM), a result consistent with the fact that calcium is involved in adipocyte TG synthesis (50) and the increased abundance of the PI 3-kinase catalytic subunit (p110 $\alpha$ ) in 3T3-L1 cells treated with AA.

Although PI 3-kinase has been identified as an absolute requirement for GLUT4 translocation in insulin-induced glucose uptake, the participation of the downstream effector Akt/protein kinase B is still debated (51). We found that phosphorylation of Akt1 on both Ser473 and Thr308 is increased by the inhibition of mitochondrial respiration. Moreover, although Akt1 phosphorylation is reduced on both residues in the presence of BAPTA-AM, Thr308 phosphorylation is far more sensitive to calcium chelation than is Ser473 phosphorylation, an observation already reported for insulin-stimulated 3T3-L1 cells (52). These results suggest that calcium is necessary for Akt1 activation triggered by AA. However, the kinase that phosphorylates Akt1 has not yet been identified. The Thr308 residue is classically phosphorylated by phosphoinositide-dependent kinase-1, but the activity of this kinase is not regulated by



calcium in insulin-stimulated 3T3-L1 cells (52). It is thus likely that calcium is able to regulate the activity of another calcium-dependent Akt1 kinase that phosphorylates the enzyme on Thr308, such as  $\text{Ca}^{2+}$ /calmodulin-dependent protein kinase II and/or  $\text{Ca}^{2+}$ /calmodulin-dependent protein kinase kinase  $\alpha$  (53).

ROS generated by impaired mitochondria also act as messengers and have recently been implicated in the inhibition of preadipocyte differentiation induced by AA (10). Even if we cannot completely rule out any participation of ROS in TG accumulation in these conditions, there is evidence supporting the fact that these messengers are not essential compared with calcium. First, neither NAC, ergothionein, nor taxifolin was able to inhibit TG accumulation in AA-incubated cells (data not shown). Furthermore, stigmatellin, another complex III inhibitor that does not generate detectable ROS (54), is also able to increase TG content in 3T3-L1 cells.

The activation of a PI 3-kinase/Akt1/GSK3 $\beta$  pathway in cells incubated with AA was also confirmed by the reduced GSK3 $\beta$  activity in cells with impaired mitochondrial respiration. GSK3 $\beta$  is known to be transiently inhibited in cells stimulated with insulin (55) and to play a role in glucose uptake. Indeed, the inhibition of GSK3 $\beta$  with lithium increases glucose uptake by a mechanism that involves a decrease of IRS-1 phosphorylation on serine residues that increases sensitivity to insulin (56). When 3T3-L1 cells were incubated with SB216763, a specific GSK3 $\beta$  inhibitor, we also observed an increase in glucose uptake for control cells but not for AA-treated cells. These data suggest that AA could already induce a maximal inhibition of GSK3 $\beta$ , as demonstrated by the *in vitro* kinase assay. Thus, this enzyme could represent the effector of the PI 3-kinase path-

way responsible for AA-induced glucose uptake in 3T3-L1 cells.


The AMPK pathway is classically activated in cells with impaired mitochondrial energetic activity (57) and controls glucose uptake mainly in muscles (32, 58, 59). AMPK is allosterically activated by AMP binding that increases AMPK kinase-dependent phosphorylation on Thr172 (60). As expected, we found a transient AMPK activation in AA-treated 3T3-L1 cells that correlates with a more sustained phosphorylation of ACC on Ser79, an observation already reported by other groups (61, 62). However, although activation of AMPK by AICAR induces a slight but not significant increase in basal glucose uptake, the overexpression of a dominant negative form of AMPK does not reduce basal or AA-stimulated glucose uptake. These results suggest that AMPK is not involved in glucose uptake in 3T3-L1 cells. Indeed, it has already been shown that AMPK activation is not involved in glucose uptake in adipocytes and that AICAR-stimulated glucose uptake in these cells does not require AMPK activity (63).

Among the mechanisms involved in glucose-mediated effects, cataplerotic reactions providing precursors for lipogenesis as well as the activation of transcription factors have been described. For example, in hepatocytes, it is known that the increase of intracellular glucose triggers the activation of ChREBP, a factor that binds the E-box in the promoter of genes involved in lipogenesis such as ACC and FAS (26). On the one hand, our data demonstrate that AA triggers the activation of ChREBP, suggesting that glucose could indirectly regulate the expression of genes involved in fatty acid synthesis. A possible role for active lipogenesis in TG accumulation in response to mitochondrial inhibition is further supported by the fact that ACC inhi-

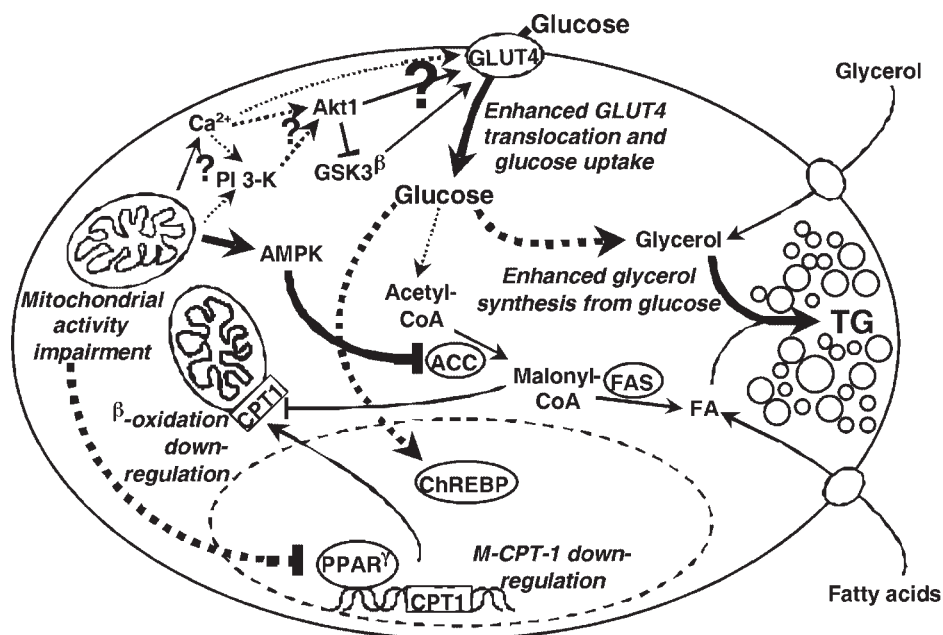


**Fig. 12.** Schematic representation of the molecular pathways leading to TG accumulation in preadipocytes with mitochondrial deficiency that involve a reduction in fatty acid  $\beta$ -oxidation and enhanced glycerol-3-phosphate synthesis from glucose. The thickness of the arrows indicates the importance of the reaction or flux. Discontinuous arrows represent multiple-step pathways.

bition by EGCG completely prevents TG accumulation in AA-treated 3T3-L1 cells. However, as ACC is phosphorylated and thus inhibited during the first 48 h of AA treatment (Fig. 9B), these results could be explained if we accept that early AMPK-mediated ACC inhibition is relieved later during AA treatment or if the AMPK-induced phosphorylation does not lead to a complete inhibition of ACC. On the other hand, we measured a  $^{14}\text{C}$ -radiolabeled glucose conversion into TG in 3T3-L1 cells incubated with AA. This is a strong argument that massive glucose uptake by 3T3-L1 preadipocytes with impaired mitochondrial activity might also enhance glycerol-3-phosphate synthesis, leading to TG accumulation.

In conclusion, this study clearly identified some new mechanisms by which a prolonged mitochondrial dysfunction triggers the accumulation of cytosolic TG in preadipocytes, leading to the acquisition of a multivesicular phenotype (summarized in Fig. 12). Although modifications in preadipocyte physiology induced by the accumulation of TG in response to mitochondrial activity impairment still have to be determined, it is interesting that adipocytes with a multivesicular phenotype have been described in some pathologies resulting from mitochondrial deficiency, such as multiple symmetric lipomatosis (7). Pathological cytosolic TG accumulation observed in muscle from MERRF patients (2, 6) might also be another manifestation of the same phenomenon. Taken together, these data contribute to a better molecular understanding of pathologies characterized by alterations of both mitochondrial activity and lipid metabolism. 

T.A. is a Research Associate of the Fonds National de la Recherche Scientifique, Belgium. S.V. is the recipient of a doctoral fellowship from the Fonds pour la Recherche dans l'Industrie et l'Agriculture. The authors thank Prof. Liao (Department of Biochemistry, Molecular Biology, and Biophysics, University of Minnesota) for the FABP4/aP2 antibody, Prof. D. Carling (Imperial College School of Medicine, Hammersmith Hospital, London, UK) for the dominant negative form of AMPK construct, and B. Spiegelman (Dana-Farber Cancer Institute, Harvard Medical School) for the PPAR $\gamma$ 2 expression vector (pSV-SPORT PPAR $\gamma$ 2). The authors are also very grateful to Prof. R. M. Evans (Howard Hughes Medical Institutes, The Salk Institute for Biological Studies) for the tk-PPREx3-Luc. The ChREBP-sensitive luciferase construct driven by the L-PK promoter was a generous gift from Dr. K. Uyeda (University of Texas Southwestern Medical Center, Dallas). This text presents results of the Belgian Program on Interuniversity Poles of Attraction initiated by the Belgian State, Prime Minister's Office Science Policy Programming. Scientific responsibility is assumed by the authors.

## REFERENCES

- Klopstock, T., M. Naumann, P. Seibel, B. Schalke, K. Reiners, and H. Reichmann. 1997. Mitochondrial DNA mutations in multiple symmetric lipomatosis. *Mol. Cell. Biochem.* **174**: 271–275.
- Munoz-Malaga, A., J. Bautista, J. A. Salazar, I. Aguilera, R. Garcia, I. Chinchon, M. D. Segura, Y. Campos, and J. Arenas. 2000. Lipomatosis, proximal myopathy, and the mitochondrial 8344 mutation. A lipid storage myopathy? *Muscle Nerve.* **23**: 538–542.
- Kakuda, T. N. 2000. Pharmacology of nucleoside and nucleotide reverse transcriptase inhibitor-induced mitochondrial toxicity. *Clin. Ther.* **22**: 685–708.
- Graeber, M. B., and U. Muller. 1998. Recent developments in the molecular genetics of mitochondrial disorders. *J. Neurol. Sci.* **153**: 251–263.
- Shoffner, J. M., M. T. Lott, A. M. Lezza, P. Seibel, S. W. Ballinger, and D. C. Wallace. 1990. Myoclonic epilepsy and ragged-red fiber disease (MERRF) is associated with a mitochondrial DNA tRNA(Lys) mutation. *Cell.* **61**: 931–937.
- Naumann, M., R. Kiefer, K. V. Toyka, C. Sommer, P. Seibel, and H. Reichmann. 1997. Mitochondrial dysfunction with myoclonus epilepsy and ragged-red fibers point mutation in nerve, muscle, and adipose tissue of a patient with multiple symmetric lipomatosis. *Muscle Nerve.* **20**: 833–839.
- Zancanaro, C., A. Sbarbati, M. Morroni, R. Carraro, M. Cigolini, G. Enzi, and S. Cinti. 1990. Multiple symmetric lipomatosis. Ultrastructural investigation of the tissue and preadipocytes in primary culture. *Lab. Invest.* **63**: 253–258.
- Klopstock, T., M. Naumann, B. Schalke, F. Bischof, P. Seibel, M. Kottlors, P. Eckert, K. Reiners, K. V. Toyka, and H. Reichmann. 1994. Multiple symmetric lipomatosis: abnormalities in complex IV and multiple deletions in mitochondrial DNA. *Neurology.* **44**: 862–866.
- Berkovic, S. F., F. Andermann, E. A. Shoubbridge, S. Carpenter, Y. Robitaille, E. Andermann, C. Melmed, and G. Karpati. 1991. Mitochondrial dysfunction in multiple symmetrical lipomatosis. *Ann. Neurol.* **29**: 566–569.
- Carriere, A., M. C. Carmona, Y. Fernandez, M. Rigoulet, R. H. Wenger, L. Penicaud, and L. Casteilla. 2004. Mitochondrial reactive oxygen species control the transcription factor CHOP-10/GADD153 and adipocyte differentiation: a mechanism for hypoxia-dependent effect. *J. Biol. Chem.* **279**: 40462–40469.
- Butow, R. A., and N. G. Avadhani. 2004. Mitochondrial signaling: the retrograde response. *Mol. Cell.* **14**: 1–15.
- Biswas, G., O. A. Adebajo, B. D. Freedman, H. K. Anandatheerthavarada, C. Vijayarathy, M. Zaidi, M. Kotlikoff, and N. G. Avadhani. 1999. Retrograde  $\text{Ca}^{2+}$  signaling in C2C12 skeletal myocytes in response to mitochondrial genetic and metabolic stress: a novel mode of inter-organelle crosstalk. *EMBO J.* **18**: 522–533.
- Arnould, T., S. Vankoningsloo, P. Renard, A. Houbion, N. Ninane, C. Demazy, J. Remacle, and M. Raes. 2002. CREB activation induced by mitochondrial dysfunction is a new signaling pathway that impairs cell proliferation. *EMBO J.* **21**: 53–63.
- Bradford, M. M. 1976. A rapid and sensitive method for the quantitation of microgram quantities of protein utilizing the principle of protein-dye binding. *Anal. Biochem.* **72**: 248–254.
- Muoio, D. M., K. Seefeld, L. A. Witters, and R. A. Coleman. 1999. AMP-activated kinase reciprocally regulates triacylglycerol synthesis and fatty acid oxidation in liver and muscle: evidence that sn-glycerol-3-phosphate acyltransferase is a novel target. *Biochem. J.* **338**: 783–791.
- Chen, Y., A. Takeshita, K. Ozaki, S. Kitano, and S. Hanazawa. 1996. Transcriptional regulation by transforming growth factor beta of the expression of retinoic acid and retinoid X receptor genes in osteoblastic cells is mediated through AP-1. *J. Biol. Chem.* **271**: 31602–31606.
- Bashan, N., E. Burdett, A. Guma, R. Sargeant, L. Tumiaty, Z. Liu, and A. Klip. 1993. Mechanisms of adaptation of glucose transporters to changes in the oxidative chain of muscle and fat cells. *Am. J. Physiol.* **264**: C430–C440.
- Mackall, J. C., A. K. Student, S. E. Polakis, and M. D. Lane. 1976. Induction of lipogenesis during differentiation in a "preadipocyte" cell line. *J. Biol. Chem.* **251**: 6462–6464.
- Winder, W. W., and B. F. Holmes. 2000. Insulin stimulation of glucose uptake fails to decrease palmitate oxidation in muscle if AMPK is activated. *J. Appl. Physiol.* **89**: 2430–2437.
- Jeukendrup, A. E. 2002. Regulation of fat metabolism in skeletal muscle. *Ann. NY Acad. Sci.* **967**: 217–235.
- Smith, S. A. 2002. Peroxisome proliferator-activated receptors and the regulation of mammalian lipid metabolism. *Biochem. Soc. Trans.* **30**: 1086–1090.
- Louet, J. F., C. Le May, J. P. Pegorier, J. F. Decaux, and J. Girard. 2001. Regulation of liver carnitine palmitoyltransferase I gene expression by hormones and fatty acids. *Biochem. Soc. Trans.* **29**: 310–316.
- Huss, J. M., F. H. Levy, and D. P. Kelly. 2001. Hypoxia inhibits the peroxisome proliferator-activated receptor alpha/retinoid X recep-

- tor gene regulatory pathway in cardiac myocytes: a mechanism for O<sub>2</sub>-dependent modulation of mitochondrial fatty acid oxidation. *J. Biol. Chem.* **276**: 27605–27612.
24. Mangelsdorf, D. J., and R. M. Evans. 1995. The RXR heterodimers and orphan receptors. *Cell.* **83**: 841–850.
25. Mercado, C. L., J. N. Loeb, and F. Ismail-Beigi. 1989. Enhanced glucose transport in response to inhibition of respiration in Clone 9 cells. *Am. J. Physiol.* **257**: C19–C28.
26. Uyeda, K., H. Yamashita, and T. Kawaguchi. 2002. Carbohydrate responsive element-binding protein (ChREBP): a key regulator of glucose metabolism and fat storage. *Biochem. Pharmacol.* **63**: 2075–2080.
27. Tsakiridis, T., M. Vranic, and A. Klip. 1994. Disassembly of the actin network inhibits insulin-dependent stimulation of glucose transport and prevents recruitment of glucose transporters to the plasma membrane. *J. Biol. Chem.* **269**: 29934–29942.
28. Whitehead, J. P., J. C. Molerio, S. Clark, S. Martin, G. Meneilly, and D. E. James. 2001. The role of Ca<sup>2+</sup> in insulin-stimulated glucose transport in 3T3-L1 cells. *J. Biol. Chem.* **276**: 27816–27824.
29. Reusch, J. E., and D. J. Klemm. 2002. Inhibition of cAMP-response element-binding protein activity decreases protein kinase B/Akt expression in 3T3-L1 adipocytes and induces apoptosis. *J. Biol. Chem.* **277**: 1426–1432.
30. Shaw, M., P. Cohen, and D. R. Alessi. 1997. Further evidence that the inhibition of glycogen synthase kinase-3beta by IGF-1 is mediated by PDK1/PKB-induced phosphorylation of Ser-9 and not by dephosphorylation of Tyr-216. *FEBS Lett.* **416**: 307–311.
31. Jope, R. S. 2003. Lithium and GSK-3: one inhibitor, two inhibitory actions, multiple outcomes. *Trends Pharmacol. Sci.* **24**: 441–443.
32. Koistinen, H. A., D. Galuska, A. V. Chibalin, J. Yang, J. R. Zierath, G. D. Holman, and H. Wallberg-Henriksson. 2003. 5-Aminoimidazole carboxamide riboside increases glucose transport and cell-surface GLUT4 content in skeletal muscle from subjects with type 2 diabetes. *Diabetes.* **52**: 1066–1072.
33. Woods, A., D. Azzout-Marniche, M. Foretz, S. C. Stein, P. Lemarchand, P. Ferre, F. Foufelle, and D. Carling. 2000. Characterization of the role of AMP-activated protein kinase in the regulation of glucose-activated gene expression using constitutively active and dominant negative forms of the kinase. *Mol. Cell. Biol.* **20**: 6704–6711.
34. Zeviani, M., A. Spinazzola, and V. Carelli. 2003. Nuclear genes in mitochondrial disorders. *Curr. Opin. Genet. Dev.* **13**: 262–270.
35. Liao, X., and R. A. Butow. 1993. RTG1 and RTG2: two yeast genes required for a novel path of communication from mitochondria to the nucleus. *Cell.* **72**: 61–71.
36. Arnould, T., L. Mercy, A. Houbion, S. Vankoningsloo, P. Renard, T. Pascal, N. Ninane, C. Demazy, and M. Raes. 2003. mtCLIC is up-regulated and maintains a mitochondrial membrane potential in mtDNA-depleted L929 cells. *FASEB J.* **17**: 2145–2147.
37. Lapsys, N. M., A. D. Kriketos, M. Lim-Fraser, A. M. Poynten, A. Lowy, S. M. Furler, D. J. Chisholm, and G. J. Cooney. 2000. Expression of genes involved in lipid metabolism correlate with peroxisome proliferator-activated receptor gamma expression in human skeletal muscle. *J. Clin. Endocrinol. Metab.* **85**: 4293–4297.
38. Kerner, J., and C. Hoppel. 2000. Fatty acid import into mitochondria. *Biochim. Biophys. Acta.* **1486**: 1–17.
39. Spiegelman, B. M., E. Hu, J. B. Kim, and R. Brun. 1997. PPAR gamma and the control of adipogenesis. *Biochimie.* **79**: 111–112.
40. Hegele, R. A., H. Cao, C. Frankowski, S. T. Mathews, and T. Leff. 2002. PPARG F388L, a transactivation-deficient mutant, in familial partial lipodystrophy. *Diabetes.* **51**: 3586–3590.
41. Mueller, E., S. Drori, A. Aiyer, J. Yie, P. Sarraf, H. Chen, S. Hauser, E. D. Rosen, K. Ge, R. G. Roeder, et al. 2002. Genetic analysis of adipogenesis through peroxisome proliferator-activated receptor gamma isoforms. *J. Biol. Chem.* **277**: 41925–41930.
42. Gulick, T., S. Cresci, T. Cairra, D. D. Moore, and D. P. Kelly. 1994. The peroxisome proliferator-activated receptor regulates mitochondrial fatty acid oxidase gene expression. *Proc. Natl. Acad. Sci. USA.* **91**: 11012–11016.
43. Brown, N. F., J. K. Hill, V. Esser, J. L. Kirkland, B. E. Corkey, D. W. Foster, and J. D. McGarry. 1997. Mouse white adipocytes and 3T3-L1 cells display an anomalous pattern of carnitine palmitoyltransferase (CPT) I isoform expression during differentiation. Inter-tissue and inter-species expression of CPT I and CPT II enzymes. *Biochem. J.* **327**: 225–231.
44. Song, S., Y. Zhang, K. Ma, L. Jackson-Hayes, E. N. Lavrentyev, G. A. Cook, M. B. Elam, and E. A. Park. 2004. Peroxisomal proliferator activated receptor gamma coactivator (PGC-1alpha) stimulates carnitine palmitoyltransferase I (CPT-1alpha) through the first intron. *Biochim. Biophys. Acta.* **1679**: 164–173.
45. Mascaro, C., E. Acosta, J. A. Ortiz, P. F. Marrero, F. G. Hegardt, and D. Haro. 1998. Control of human muscle-type carnitine palmitoyltransferase I gene transcription by peroxisome proliferator-activated receptor. *J. Biol. Chem.* **273**: 8560–8563.
46. Owen, O. E., S. C. Kalhan, and R. W. Hanson. 2002. The key role of anaplerosis and cataplerosis for citric acid cycle function. *J. Biol. Chem.* **277**: 30409–30412.
47. Kang, J., E. Heart, and C. K. Sung. 2001. Effects of cellular ATP depletion on glucose transport and insulin signaling in 3T3-L1 adipocytes. *Am. J. Physiol. Endocrinol. Metab.* **280**: E428–E435.
48. Hamrahian, A. H., J. Z. Zhang, F. S. Elkhairi, R. Prasad, and F. Ismail-Beigi. 1999. Activation of Glut1 glucose transporter in response to inhibition of oxidative phosphorylation. *Arch. Biochem. Biophys.* **368**: 375–379.
49. Patel, N., Z. A. Khayat, N. B. Ruderman, and A. Klip. 2001. Dissociation of 5' AMP-activated protein kinase activation and glucose uptake stimulation by mitochondrial uncoupling and hyperosmolar stress: differential sensitivities to intracellular Ca<sup>2+</sup> and protein kinase C inhibition. *Biochem. Biophys. Res. Commun.* **285**: 1066–1070.
50. Zemel, M. B. 1998. Nutritional and endocrine modulation of intracellular calcium: implications in obesity, insulin resistance and hypertension. *Mol. Cell. Biochem.* **188**: 129–136.
51. Salt, I. P., J. M. Connell, and G. W. Gould. 2000. 5-Aminoimidazole-4-carboxamide ribonucleoside (AICAR) inhibits insulin-stimulated glucose transport in 3T3-L1 adipocytes. *Diabetes.* **49**: 1649–1656.
52. Worrall, D. S., and J. M. Olefsky. 2002. The effects of intracellular calcium depletion on insulin signaling in 3T3-L1 adipocytes. *Mol. Endocrinol.* **16**: 378–389.
53. Okuno, S., T. Kitani, H. Matsuzaki, H. Konishi, U. Kikkawa, and H. Fujisawa. 2000. Studies on the phosphorylation of protein kinase B by Ca(2+)/calmodulin-dependent protein kinases. *J. Biochem. (Tokyo).* **127**: 965–970.
54. Raha, S., G. E. McEachern, A. T. Myint, and B. H. Robinson. 2000. Superoxides from mitochondrial complex III: the role of manganese superoxide dismutase. *Free Radic. Biol. Med.* **29**: 170–180.
55. Cross, D. A., D. R. Alessi, P. Cohen, M. Andjelkovich, and B. A. Hemmings. 1995. Inhibition of glycogen synthase kinase-3 by insulin mediated by protein kinase B. *Nature.* **378**: 785–789.
56. Orena, S. J., A. J. Torchia, and R. S. Garofalo. 2000. Inhibition of glycogen-synthase kinase 3 stimulates glycogen synthase and glucose transport by distinct mechanisms in 3T3-L1 adipocytes. *J. Biol. Chem.* **275**: 15765–15772.
57. Hardie, D. G. 1999. Roles of the AMP-activated/SNF1 protein kinase family in the response to cellular stress. *Biochem. Soc. Symp.* **64**: 13–27.
58. Fryer, L. G., F. Foufelle, K. Barnes, S. A. Baldwin, A. Woods, and D. Carling. 2002. Characterization of the role of the AMP-activated protein kinase in the stimulation of glucose transport in skeletal muscle cells. *Biochem. J.* **363**: 167–174.
59. Musi, N., and L. J. Goodyear. 2003. AMP-activated protein kinase and muscle glucose uptake. *Acta Physiol. Scand.* **178**: 337–345.
60. Hawley, S. A., M. Davison, A. Woods, S. P. Davies, R. K. Beri, D. Carling, and D. G. Hardie. 1996. Characterization of the AMP-activated protein kinase kinase from rat liver and identification of threonine 172 as the major site at which it phosphorylates AMP-activated protein kinase. *J. Biol. Chem.* **271**: 27879–27887.
61. Tomas, E., T. S. Tsao, A. K. Saha, H. E. Murrey, Cc. Zhang, S. I. Itani, H. F. Lodish, and N. B. Ruderman. 2002. Enhanced muscle fat oxidation and glucose transport by ACRP30 globular domain: acetyl-CoA carboxylase inhibition and AMP-activated protein kinase activation. *Proc. Natl. Acad. Sci. USA.* **99**: 16309–16313.
62. Rasmussen, B. B., C. R. Hancock, and W. W. Winder. 1998. Postexercise recovery of skeletal muscle malonyl-CoA, acetyl-CoA carboxylase, and AMP-activated protein kinase. *J. Appl. Physiol.* **85**: 1629–1634.
63. Sakoda, H., T. Ogihara, M. Anai, M. Fujishiro, H. Ono, Y. Onishi, H. Katagiri, M. Abe, Y. Fukushima, N. Shojima, et al. 2002. Activation of AMPK is essential for AICAR-induced glucose uptake by skeletal muscle but not adipocytes. *Am. J. Physiol. Endocrinol. Metab.* **282**: E1239–E1244.